Journal of Computational Physics 229 (2010) 851–874

Contents lists available at ScienceDirect

Journal of Computational Physics

journal homepage: www.elsevier.com/locate/jcp

Improved transmission conditions for a one-dimensional domain decomposition method applied to the solution of the Helmholtz equation

Bruno Stupfel *

CEA, DAM, CESTA, F-33114 Le Barp, France

ARTICLE INFO

Article history:
Received 23 January 2009
Received in revised form 15 September 2009
Accepted 10 October 2009
Available online 20 October 2009

Keywords:
Electromagnetism
Helmholtz equation
Frequency domain
Domain decomposition method
Transmission conditions
Numerical methods

ABSTRACT

The scattering problem of a time-harmonic electromagnetic wave from a perfect electric conductor (PEC) coated with materials is considered, and solved by coupling a finite element method with an integral equation prescribed on the outer boundary of the computational domain. To reduce the numerical complexity, a one-dimensional domain decomposition method (DDM) is employed: the computational domain is partitioned into concentric subdomains (SDs), and Robin transmission conditions (TCs) are prescribed on the interfaces. For some configurations and/or materials, the convergence of the corresponding DDM algorithm happens to be slow. A possible remedy is to enhance the efficiency of the TCs by approximating the exact ones more accurately. To this end, we first consider the simplified 2D problem of a circular PEC cylinder with an homogeneous coating and up to four SDs with circular interfaces, thus allowing to obtain the exact TCs in closed-form. Approximate local or non-local TCs are derived from these exact ones, and numerical examples demonstrate their superiority over the standard Robin TCs. Then, the case of an elliptical PEC cylinder with one interface in free-space is investigated. Also, the issues pertaining to the uniqueness of the solutions and convergence of the algorithm are addressed.

1. Introduction

The scattering problem of a time-harmonic electromagnetic wave from complex 3D inhomogeneous objects embedded in free-space can be accurately solved by coupling a finite element method (FEM) with an integral equation (IE) prescribed on the outer boundary of the computational domain. For electrically large objects, a domain decomposition method (DDM) allows a considerable reduction of its numerical complexity by decomposing the initial problem into several coupled subproblems that are solved independently. Such an hybrid DDM has been presented in [1–3] that is based, essentially, on the DDM proposed by Després et al. [4]: the subdomains (SDs) are coupled via a Robin transmission condition (TC) that ensures the uniqueness of the solutions and the convergence of the iterative algorithm. In [1,2], the convergence is accelerated by partitioning the computational domain into concentric SDs (onion-like partition), and Després' DDM algorithm has been modified accordingly. However, for a perfect electric conductor (PEC) coated with materials, it may happen that this algorithm converges rapidly when the first (innermost) interface is located in free-space only. For an electrically large object and high index materials, this entails a prohibitively large number of volume unknowns inside the first SD.

A possible way to overcome this problem is to employ FETI-like methods [5–13]: the interior unknowns in each SD are eliminated by performing a Schur complement, and only the resulting system with the unknowns on the interfaces between the SDs is considered. This allows a reduction of the memory size and the use of a Krylov iterative solver. However, the size of

* Tel.: +33 05 57 04 50 10.
E-mail address: bruno.stupfel@cea.fr

0021-9991/$ - see front matter © 2009 Elsevier Inc. All rights reserved.
doi:10.1016/j.jcp.2009.10.015

this system may still be very large, preconditioning is generally necessary, and uniqueness of the solutions is not always guaranteed. Another possibility is to enhance the performances of Després' original TCs. Without pretending to be exhaustive, we may mention numerical TCs [8,18], second order TCs – that involve second order tangential derivatives of the fields on the interfaces – [15,7,16,23], and zero order TCs defined for the two following model problems: unbounded homogeneous medium with a planar interface [17,23], and a 2D coated PEC circular cylinder with one circular interface located in free-space [19], the solution of which is also easily obtained in closed-form. In both cases, Després' algorithm only is considered.

In this paper, we complexify the latter 2D model by adding one or two interfaces inside the coating, in order to approach more closely a real-world problem. Besides, the onion-like (1D) DDM algorithm [15] is employed, that is known to converge more rapidly than the one originally proposed by Després. The model problem with two interfaces is presented in Section 2, together with the definitions of the exact TCs, of the global system reduced to the unknowns on the interface, and of the radius of convergence of the algorithm. The performances of the approximate TCs proposed, e.g., in [17,19] are investigated in Section 3, as well as those of the relaxed algorithm in [15]; also, the issues pertaining to the uniqueness of the solutions and convergence of the algorithm are addressed. More efficient TCs are presented and numerically evaluated in Section 4, and the influence of an additional TC on the convergence is investigated in Section 5. The case of an elliptical PEC cylinder with two free-space subdomains only is investigated in Section 6, and conclusions are proposed in Section 7.

2. Model problem: 2D circular cylinders

We consider the 2D geometry (translationally invariant along z) sketched in Fig. 1. It is embedded in free-space and illuminated by the plane wave $u^{inc} = e^{ik_0 x}$ where $k_0 = 2\pi f/c$ is the free-space wave number (c is the light velocity), and the time dependence $\exp(2i\pi ft)$ is assumed and suppressed throughout. The Helmholtz equation $\Delta u + k^2 u = 0$ is solved with an exact radiation condition at infinity – for example an IE – and $k = k_0\sqrt{\epsilon\mu}$ where ϵ, μ are the relative permittivity and permeability of the material, being both equal to one in free-space. S_0 is the surface of a PEC:

$$\text{TM}: \ u(S_0) = 0; \quad \text{TE}: \ \partial_n u(S_0) = 0 \tag{1}$$

u is the total field, equal to E_z ($\eta_0 H_z$) in TM (respectively TE) polarization ($\underline{E}$, $\underline{H}$ are the electric and magnetic fields and η_0 is the free-space impedance); ∂_n stands for $\underline{n}.\underline{\nabla}$ where $\underline{n}$ is the outward normal to S_0. This problem is representative of a real-world one: a TC on S1 inside the material and another one on S3 for the hybridization with the IE in free-space [1,2]. An additional interface located inside the material will be considered in Section 5. A general solution of the Helmholtz equation in polar coordinates is

$$u(r,\theta) = \sum_{m=-\infty}^{+\infty} [a_m J_m(kr) + b_m H_m(kr)] e^{im\theta} \tag{2}$$

where $J_m(x), H_m(x) \equiv H_m^{(2)}(x)$ are the Bessel and Hankel functions of order m, and $k = k_0$ for $r \geqslant R_2$. Note that $e^{ik_0 x} = \sum_{m=-\infty}^{+\infty} i^m J_m(k_0 r) e^{im\theta}$ implies

$$a_{-m} = (-1)^m a_m \quad b_{-m} = (-1)^m b_m \tag{3}$$

2.1. Exact solution

The coefficients for the exact solution that will serve as a reference are:

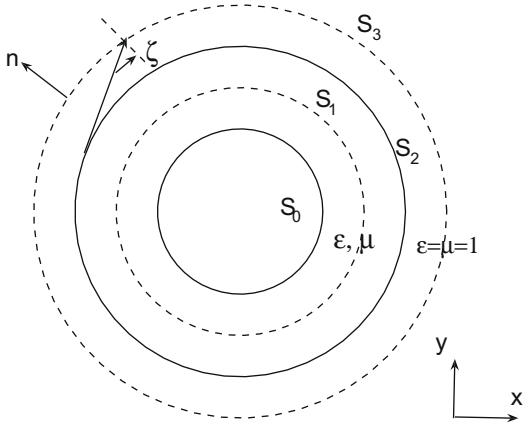

Fig. 1. R_i is the radius of circle S_i, $0 \leqslant i \leqslant 3$. S_0 is a PEC surface; ϵ and μ are constant for $R_0 \leqslant r \leqslant R_2$ and $\epsilon = \mu = 1$ for $r \geqslant R_2$. TCs are prescribed on S_1 and S_3. The normals $\underline{n}$ to the circles are all oriented outward. The arrow represents a ray tangent to S_2 and incident on S_3 with the angle ζ (see Section 4.1.4).

$$\begin{aligned} &R_0 \leqslant r \leqslant R_2: \quad b_m^{ex} = -\frac{2i^{m+1}}{\pi k_0 R_2 \varphi_m \chi_m (1-\tau_m)};\ a_m^{ex} = -\varphi_m b_m^{ex} \\ &r \geqslant R_2: \quad b_m^{ex} = \frac{i^m \delta'_m (1-\tau'_m)}{\varphi_m \chi_m (1-\tau_m)};\ a_m^{ex} = i^m \end{aligned} \tag{4}$$

where

$$\begin{aligned} &\text{TM}: \ \varphi_m = \frac{H_m(kR_0)}{J_m(kR_0)}; \quad \text{TE}: \ \varphi_m = \frac{H'_m(kR_0)}{J'_m(kR_0)} \\ &J'_m(x) = \frac{d}{dx} J_m(x); \quad H'_m(x) = \frac{d}{dx} H_m(x) \end{aligned} \tag{5}$$

and, in TE:

$$\begin{aligned} &\chi_m = \eta J'_m(kR_2) H_m(k_0 R_2) - J_m(kR_2) H'_m(k_0 R_2); \quad \eta = \sqrt{\mu/\epsilon} \\ &\chi'_m = \eta J'_m(kR_2) J_m(k_0 R_2) - J_m(kR_2) J'_m(k_0 R_2) \\ &\delta_m = \eta H'_m(kR_2) H_m(k_0 R_2) - H_m(kR_2) H'_m(k_0 R_2) \\ &\delta'_m = \eta H'_m(kR_2) J_m(k_0 R_2) - H_m(kR_2) J'_m(k_0 R_2) \\ &\tau_m = \frac{\delta_m}{\varphi_m \chi_m}; \quad \tau'_m = \frac{\varphi_m \chi'_m}{\delta'_m} \end{aligned} \tag{6}$$

The corresponding formulas in TM are obtained from (6) by interchanging ϵ and μ (then η is replaced by $1/\eta$); this rule applies in all what follows.

2.2. Exact transmission conditions. Global system reduced to the unknowns on the interfaces

The DDM algorithm in [2] writes, at iteration ℓ,

$$\begin{aligned} S_1: \quad & T^+ u_1^\ell = (1-\omega_\ell) T^+ u_1^{\ell-1} + \omega_\ell T^+ u_2^{\ell-1} \\ & T^- u_2^\ell = T^- u_1^\ell \\ S_3: \quad & T^+ u_3^\ell = (1-\omega_\ell) T^+ u_3^{\ell-1} + \omega_\ell T^+ u_4^{\ell-1} \\ & T^- u_4^\ell = T^- u_3^\ell \end{aligned} \tag{7}$$

ω_ℓ is the relaxation parameter ($1/2 \leqslant \omega_\ell \leqslant 1$), $T^\pm$ are the operators that define the TCs, and u_i, $1 \leqslant i \leqslant 4$, designate the solutions for $R_{i-1} \leqslant r \leqslant R_i$ ($R_4 = \infty$). In [2], $T^\pm$ are identical on all the interfaces and write, in TE,

$$T^\pm u = \frac{\partial_n u}{\epsilon} \pm i k_0 u \tag{8}$$

($\epsilon = 1$ on S_3). These approximate TCs (termed henceforth standard TCs) guarantee the convergence [14] that may happen to be slow, as mentioned in Section 1. It is accelerated via a better approximation of the exact TCs. An exact TC is a non-local operator than can be defined as follows (in TE):

$$\begin{aligned} &T^\pm u = \partial_n u/\epsilon \pm Z^\pm u; \quad Z^\pm u(\theta) = \frac{1}{2\pi} \int_0^{2\pi} Z^\pm(\theta, \theta') u(\theta') d\theta' \\ &Z^\pm(\theta, \theta') = \sum_{m=-\infty}^{+\infty} v_m^\pm e^{im(\theta-\theta')} \end{aligned} \tag{9}$$

Because u is given by (2), we get $Z^\pm u(\theta) = \sum_{m=-\infty}^{+\infty} v_m^\pm [a_m J_m(kr) + b_m H_m(kr)] e^{im\theta}$ for $r = R_1, R_3$. Since $\partial_n u(\theta)/\epsilon = k_0 \eta \sum_{m=-\infty}^{+\infty} [a_m J'_m(kr) + b_m H'_m(kr)] e^{im\theta}$, the exact TCs in (7) write:

$$\begin{aligned} S_1: \quad & a_{1m}^\ell + \psi_{1m}^+ b_{1m}^\ell = (1-\omega_\ell)(a_{1m}^{\ell-1} + \psi_{1m}^+ b_{1m}^{\ell-1}) + \omega_\ell (a_{2m}^{\ell-1} + \psi_{1m}^+ b_{2m}^{\ell-1});\ a_{2m}^\ell + \psi_{1m}^- b_{2m}^\ell = a_{1m}^\ell + \psi_{1m}^- b_{1m}^\ell \\ S_3: \quad & a_{3m}^\ell + \psi_{3m}^+ b_{3m}^\ell = (1-\omega_\ell)(a_{3m}^{\ell-1} + \psi_{3m}^+ b_{3m}^{\ell-1}) + \omega_\ell (i^m + \psi_{3m}^+ b_{4m}^{\ell-1});\ i^m + \psi_{3m}^- b_{4m}^\ell = a_{3m}^\ell + \psi_{3m}^- b_{3m}^\ell \end{aligned} \tag{10}$$

where

$$\psi_{1m}^\pm = \frac{\eta H'_m(kR_1) \pm \frac{v_{1m}^\pm}{k_0} H_m(kR_1)}{\eta J'_m(kR_1) \pm \frac{v_{1m}^\pm}{k_0} J_m(kR_1)} \quad \psi_{3m}^\pm = \frac{H'_m(k_0 R_3) \pm \frac{v_{3m}^\pm}{k_0} H_m(k_0 R_3)}{J'_m(k_0 R_3) \pm \frac{v_{3m}^\pm}{k_0} J_m(k_0 R_3)} \tag{11}$$

In (10), because of the exact radiation condition, we have used the fact that coefficient a_{4m} in (2) is the one, i^m, of the incident wave. For the standard TCs, we have, in view of (8),

$$v_m^+ = v_m^- = i k_0 \quad \forall m \tag{12}$$

To obtain the global system reduced to the unknowns on the interfaces, the continuity of the tangential components of $\underline{E}$ and $\underline{H}$ must be enforced on S_2, viz., in 2D-TE, the continuity of u and $\partial_n u/\epsilon$ for $r = R_2$ that yields:

$$\begin{aligned} &a_{2m}\alpha_m + b_{2m} - a_{3m}\beta_m - b_{3m}\gamma_m = 0 \quad a_{2m}\alpha'_m + b_{2m} - a_{3m}\beta'_m - b_{3m}\gamma'_m = 0 \\ &\alpha_m = \frac{J_m(kR_2)}{H_m(kR_2)} \quad \alpha'_m = \frac{J'_m(kR_2)}{H'_m(kR_2)} \quad \beta_m = \frac{J_m(k_0R_2)}{H_m(kR_2)} \quad \beta'_m = \frac{J'_m(k_0R_2)}{\eta H'_m(kR_2)} \\ &\gamma_m = \frac{H_m(k_0R_2)}{H_m(kR_2)} \quad \gamma'_m = \frac{H'_m(k_0R_2)}{\eta H'_m(kR_2)} \end{aligned} \tag{13}$$

(1) implies $a_{1m} = -b_{1m}\varphi_m$. Introducing vectors $\underline{u}_m = (b_{1m}, a_{1m}, b_{2m}, a_{2m}, b_{3m}, a_{3m}, b_{4m})^t$ and $\underline{f}_m = (0,0,0,0,0,0,i^m,i^m)^t$ then, when $\omega_\ell = 1$, the global system with the unknowns on the interfaces obtained from (10) – where the coefficients are ℓ independent – and (13) writes $\mathbf{A}\underline{U} = \underline{F}$ where $\mathbf{A}$ is block-diagonal and $\underline{u}_m$, $\underline{f}_m$ are the components of $\underline{U}$, $\underline{F}$:

$$\mathbf{A}_m\underline{u}_m = \underline{f}_m \quad \forall m \tag{14}$$

with

$$\mathbf{A}_m = \begin{pmatrix} \varphi_m & 1 & 0 & 0 & 0 & 0 & 0 \\ \psi^+_{1m} & 1 & -\psi^+_{1m} & -1 & 0 & 0 & 0 \\ \psi^-_{1m} & 1 & -\psi^-_{1m} & -1 & 0 & 0 & 0 \\ 0 & 0 & 1 & \alpha_m & -\gamma_m & -\beta_m & 0 \\ 0 & 0 & 1 & \alpha'_m & -\gamma'_m & -\beta'_m & 0 \\ 0 & 0 & 0 & 0 & \psi^+_{3m} & 1 & -\psi^+_{3m} \\ 0 & 0 & 0 & 0 & \psi^-_{3m} & 1 & -\psi^-_{3m} \end{pmatrix} \tag{15}$$

(14) yields the exact solution if:

$$\det(\mathbf{A}_m) = (\psi^-_{3m} - \psi^+_{3m})(\psi^+_{1m} - \psi^-_{1m})[\varphi_m(\alpha_m\gamma'_m - \alpha'_m\gamma_m) + \gamma_m - \gamma'_m] \neq 0 \quad \forall m \tag{16}$$

2.3. Solution of the global system by the DDM algorithm

If $\omega_\ell = \omega$ is ℓ independent, then (10) is obtained if we set

$$\mathbf{A}_m = \mathbf{M}_m - \mathbf{N}_m \quad \underline{u}^\ell_m = \mathbf{M}^{-1}_m\mathbf{N}_m\underline{u}^{\ell-1}_m + \mathbf{M}^{-1}_m\underline{f}_m \tag{17}$$

with:

$$\mathbf{M}_m = \begin{pmatrix} \varphi_m & 1 & 0 & 0 & 0 & 0 & 0 \\ \psi^+_{1m}/\omega & 1/\omega & 0 & 0 & 0 & 0 & 0 \\ \psi^-_{1m} & 1 & -\psi^-_{1m} & -1 & 0 & 0 & 0 \\ 0 & 0 & 1 & \alpha_m & -\gamma_m & -\beta_m & 0 \\ 0 & 0 & 1 & \alpha'_m & -\gamma'_m & -\beta'_m & 0 \\ 0 & 0 & 0 & 0 & \psi^+_{3m}/\omega & 1/\omega & 0 \\ 0 & 0 & 0 & 0 & \psi^-_{3m} & 1 & -\psi^-_{3m} \end{pmatrix} \tag{18}$$

$$\mathbf{N}_m = \begin{pmatrix} 0 & 0 & 0 & 0 & 0 & 0 & 0 \\ \psi^+_{1m}(1/\omega - 1) & (1/\omega - 1) & \psi^+_{1m} & 1 & 0 & 0 & 0 \\ 0 & 0 & 0 & 0 & 0 & 0 & 0 \\ 0 & 0 & 0 & 0 & 0 & 0 & 0 \\ 0 & 0 & 0 & 0 & 0 & 0 & 0 \\ 0 & 0 & 0 & 0 & \psi^+_{3m}(1/\omega - 1) & (1/\omega - 1) & \psi^+_{3m} \\ 0 & 0 & 0 & 0 & 0 & 0 & 0 \end{pmatrix} \tag{19}$$

When $\omega = 1$, this is equivalent to a block Gauss–Seidel iterative solution of (14). The problem is well posed if

$$\det(\mathbf{M}_m) = \frac{\psi^+_{1m} - \varphi_m}{\omega^2}(r^+_{om} - \psi^-_{1m}r^+_m)\psi^-_{3m} \neq 0 \quad \forall m \tag{20}$$

where

$$r^\pm_{om} = \gamma_m - \gamma'_m + \psi^\pm_{3m}(\beta'_m - \beta_m) \quad r^\pm_m = \alpha'_m\gamma_m - \alpha_m\gamma'_m + \psi^\pm_{3m}(\alpha_m\beta'_m - \alpha'_m\beta_m) \tag{21}$$

The algorithm converges if and only if

$$\rho = \max_m \rho_m < 1 \quad \rho_m = \max|\lambda_m| \tag{22}$$

where λ_m is an eigenvalue of $\mathbf{M}_m^{-1}\mathbf{N}_m$. In this case, and if the initial solution is set to zero ($\underline{u}_m^0 = 0$ for all m), we have:

$$\underline{u}_m^\ell = \sum_{n=0}^{\ell-1}(\mathbf{M}_m^{-1}\mathbf{N}_m)^n\mathbf{M}_m^{-1}\underline{f}_m \Rightarrow \underline{u}_m^\infty = \underline{u}_m = (\mathbf{I}-\mathbf{M}_m^{-1}\mathbf{N}_m)^{-1}\mathbf{M}_m^{-1}\underline{f}_m \tag{23}$$

(17) implies $\mathbf{M}_m^{-1}\mathbf{A}_m = \mathbf{I} - \mathbf{M}_m^{-1}\mathbf{N}_m$, the eigenvalues of which are $1-\lambda_m$. By definition, the TCs in (9) that are exact for (17) are such that $\rho = 0$. In this case, the eigenvalues of $\mathbf{M}_m^{-1}\mathbf{A}_m$ are equal to 1 for all m, and $\mathbf{M}$ constitutes an excellent preconditioner for the solution of the global system $\mathbf{A}\underline{U} = \underline{F}$ via a Krylov iterative method.

The difference between u_1^ℓ and u_2^ℓ on S_1 tends asymptotically to zero like ρ^ℓ:

$$\ell \to \infty: \quad err_1^\ell = \sqrt{\int_0^{2\pi}|u_1^\ell(R_1,\theta) - u_2^\ell(R_1,\theta)|^2 d\theta} \propto \rho^\ell \tag{24}$$

The geometric convergence becomes arithmetic when ρ is very close to 1: $\rho^\ell \simeq 1-\ell(1-\rho)$, thus explaining the possibly slow convergence mentioned in Section 1 of the standard algorithm with (12).

When $\omega = 1$ (no relaxation), the non-zero λ_m write:

$$\begin{aligned}
&\lambda_m = \frac{-b \pm \sqrt{b^2-4ac}}{2a}\\
&a = \psi_{3m}^-(\varphi_m - \psi_{1m}^+)(\psi_{1m}^- r_m^+ - r_{om}^+)\\
&b = \psi_{3m}^+(\varphi_m - \psi_{1m}^+)(r_{om}^- - \psi_{1m}^- r_m^-) + \psi_{3m}^-(\varphi_m - \psi_{1m}^-)(r_{om}^+ - \psi_{1m}^+ r_m^+)\\
&c = \psi_{3m}^+(\varphi_m - \psi_{1m}^-)(\psi_{1m}^+ r_m^- - r_{om}^-)
\end{aligned} \tag{25}$$

As a consequence, $\rho = 0$ if, for all m, $c = b = 0$ and $a \neq 0$ – (16) and (20) must also be verified – that entail the following expressions for coefficients $v_m^\pm$ in the exact TCs (then the algorithm converges in three iterations, i.e. the number of SDs):

$$S_3: \quad \psi_{3m}^+ = 0 \neq \psi_{3m}^- \Longleftrightarrow v_{3m}^+ = -k_0\frac{H_m'(kR_1)}{H_m(kR_1)} \tag{26}$$

and

$$\begin{aligned}
S_1: \quad &\psi_{1m}^- = \varphi_m \neq \psi_{1m}^+ \Longleftrightarrow v_{1m}^- = k_0\eta\frac{J_m'(kR_1) - H_m'(kR_1)/\varphi_m}{J_m(kR_1) - H_m(kR_1)/\varphi_m}\\
&\psi_{1m}^+ = r_m^\infty \neq \psi_{1m}^- \Longleftrightarrow v_{1m}^+ = -k_0\eta\frac{H_m'(kR_1) - J_m'(kR_1)r_m^\infty}{H_m(kR_1) - J_m(kR_1)r_m^\infty}
\end{aligned} \tag{27}$$

with

$$r_m^\infty = \frac{\gamma_m - \gamma_m'}{\alpha_m'\gamma_m - \alpha_m\gamma_m'} \tag{28}$$

Only one of the two conditions in (27) must be satisfied. $\psi_{3m}^+ = 0 \neq \psi_{3m}^-$ yields an exact TC on S_3 since we get from (10) where $\omega_\ell = 1$:

$$\psi_{3m}^+ = 0 \neq \psi_{3m}^- \Rightarrow a_{3m}^\ell = i^m, \quad b_{3m}^\ell = b_{4m}^\ell \Rightarrow u_3^\ell = u_4^\ell, \quad \partial_n u_3^\ell = \partial_n u_4^\ell \tag{29}$$

Similarly, $\psi_{1m}^- = \varphi_m \neq \psi_{1m}^+$ or $\psi_{1m}^+ = r_m^\infty \neq \psi_{1m}^-$ yields an exact TC on S_1. Note that (26) is satisfied if $R_3 = \infty$ and $v_{3m}^+ = v_{3m}^- = ik_0$ for, if $|m|$ is bounded,

$$|m| \leqslant Q: \ \lim_{R_3\to\infty}[H_m'(k_0R_3) + iH_m(k_0R_3)] = 0 \Rightarrow \lim_{R_3\to\infty}\psi_{3m}^+ = 0 \tag{30}$$

Also, we note that v_m^+ and v_m^-, and hence T^+ and T^-, are polarization dependent, that implies anisotropic TCs.

We easily get from (25) the expressions of λ_m in the two following particular cases:

- exact TC on S_3:

$$\psi_{3m}^+ = 0 \Longleftrightarrow \lambda_m = \frac{(\psi_{1m}^- - \varphi_m)(\psi_{1m}^+ - r_m^\infty)}{(\psi_{1m}^+ - \varphi_m)(\psi_{1m}^- - r_m^\infty)} \tag{31}$$

- exact TC on S_1:

$$\psi_{1m}^- = \varphi_m \Longleftrightarrow \lambda_m = \frac{\psi_{3m}^+(\varphi_m r_m^- - r_{om}^-)}{\psi_{3m}^-(\varphi_m r_m^+ - r_{om}^+)} \tag{32}$$

The latter case is the model problem considered in [19] – only one TC on S_3 – for the convergence of the non-relaxed ($\omega = 1$) Després' algorithm [14] that writes

$$T^+u_3^\ell = T^+u_4^{\ell-1} \quad T^-u_4^\ell = T^-u_3^{\ell-1}$$

and the corresponding non-zero eigenvalues are $\pm\sqrt{\lambda_m}$: we thus verify that this algorithm converges less rapidly than the one in (7).

Note that (31) and (32) can also be obtained if we proceed as in Section 2.3: the corresponding matrix $\mathbf{A}_m$ contains solely the unknowns on both sides of S_1 ($b_{1m}, a_{1m}, b_{2m}, a_{2m}$), or of S_3 (b_{3m}, a_{3m}, b_{4m}).

3. $v_m^+ = v_m^- = v$ for the TCs on S_1 and S_3

Setting $v_m^+ = v_m^-$ and m independent [$v_{1m}^+ = v_{\bar{1}m}^- = v_1$, $v_{3m}^+ = v_{\bar{3}m}^- = v_3$ in (11)] is a simple option – the only one considered in [17,19]. Unlike the standard ones in (12), these coefficients may have a non-zero real part: $v = v' + iv''$ with $v', v'' \in \mathbb{R}$. Actually, it is known (see e.g. [17]) that $v' \neq 0$ allows to act on evanescent waves that exist, for example, in the vicinity of a PEC surface.

3.1. Simplified model problem: convergence of the DDM and uniqueness of the solutions in each SD

The problem is simplified as follows (see Fig. 1): S_3 is suppressed and an absorbing boundary condition (ABC) is prescribed on S_2:

$$T^+u_2 = \partial_n u_2 + v_1 u_2 = T^+u^{inc} \tag{33}$$

In this section, S_0, S_1 and S_2 have arbitrary shapes. It follows that the Helmholtz equation is solved inside the material only, and u_1, u_2 are the solutions on each side of S_1 on which are prescribed the TCs defined by the two first identities in (7), with

$$\text{TE}: \quad T^\pm = \frac{\partial_n}{\epsilon} \pm v_1 \tag{34}$$

and $\omega_\ell = \omega \in \mathbb{C}$. Adapting the proof in [14] to the algorithm in (7), we get in Appendix A, if $e_i^\ell = u_i^\ell - u^{ex}$ where u^{ex} is the exact solution of this problem ($\Re$ and $\Im$ stand for real and imaginary parts) and $\underline{E}_i^\ell, \underline{H}_i^\ell$ designate the difference with the exact fields of the fields computed at iteration ℓ:

$$\begin{aligned}
&E^\ell = \int_{S_1} |T^+e_1^\ell|^2 + \int_{S_2} |T^+e_2^\ell|^2 = \int_{S_1} |T^+e_1^\ell|^2 \\
&E^\ell \leqslant (|\omega|^2 + |1-\omega|^2)E^{\ell-1} - |\omega|^2\left[v_1''B''^{\ell-1} + v_1'B'^{\ell-1} + 4|v_1|^2\int_{S_2}|e_2^{\ell-1}|^2\right] \\
&\omega = 1: \quad E^\ell = E^{\ell-1} - \left[v_1''B''^{\ell-1} + v_1'B'^{\ell-1} + 4|v_1|^2\int_{S_2}|e_2^{\ell-1}|^2\right] \\
&B'^\ell = \Re(B^\ell) \quad B''^\ell = \Im(B^\ell) \quad B^\ell = 4(A_1^\ell + A_2^\ell) \\
&i = 1,2: \quad A_i^\ell = k_0^2\int_{\Omega_i}[\epsilon^*|\underline{E}_i^\ell|^2 - \mu|\underline{H}_i^\ell|^2]; \quad \Im(\epsilon), \Im(\mu) \leqslant 0 \Rightarrow B''^\ell \geqslant 0
\end{aligned} \tag{35}$$

In the first identity, $\int_{S_2}|T^+e_2^\ell|^2 = 0$ because both u_2^ℓ and u^{ex} satisfy (33). Also, Ω_1 (Ω_2) is the SD bounded by S_0 and S_1 (respectively S_1 and S_2).

Regarding uniqueness conditions, Maxwell's equations are solved in Ω_1 (Ω_2) with (1) and the first identity in (7) (respectively (33) and the second identity in (7)) as boundary conditions. Uniqueness of the solutions is guaranteed if $u_i^\ell = 0$ when the r.h.s. are zero, viz. $T^+u_1^\ell = 0$ for u_1 and $T^-u_2^\ell = 0$ for u_2, and (34) writes on S_1: $\partial_n u_1^\ell/\epsilon = -v_1u_1^\ell$ and $\partial_n u_2^\ell/\epsilon = v_1u_2^\ell$. Then, we obtain from (81), with $e_i^\ell = u_i^\ell$:

$$\begin{aligned}
&k_0^2\int_{\Omega_1}[\epsilon^*|\underline{E}_1^\ell|^2 - \mu|\underline{H}_1^\ell|^2] + v_1\int_{S_1}|u_1^\ell|^2 = 0 \\
&k_0^2\int_{\Omega_2}[\epsilon^*|\underline{E}_2^\ell|^2 - \mu|\underline{H}_2^\ell|^2] + v_1\left(\int_{S_1}|u_2^\ell|^2 + \int_{S_2}|u_2^\ell|^2\right) = 0
\end{aligned} \tag{36}$$

Since $\Im(\epsilon), \Im(\mu) \leqslant 0$, taking the imaginary part of these expressions yields:

$$v_1'' \geqslant 0 \Rightarrow u_1^\ell = u_2^\ell = 0 \tag{37}$$

If $v_1' = 0$ and $v_1'' \geqslant 0$, (35) shows that $|\omega|^2 + |1-\omega|^2 \leqslant 1$ is a sufficient condition of convergence

$$\omega = \omega' + i\omega'' \in \mathbb{D} = \{(\omega' - 1/2)^2 + \omega''^2 \leqslant 1/4\} \Rightarrow E^\ell < E^{\ell-1} \tag{38}$$

and the DDM converges all the faster since losses ($B''^{\ell} > 0$) are large: then, it may be advantageous to maximize $|\omega|^2$ with $|\omega|^2 + |1-\omega|^2 \leqslant 1$, and numerical examples performed on this model problem show that $\omega = 1$ is a good trade-off.

If $v_1' \neq 0$ and $v_1'' \geqslant 0$, we cannot conclude, except when $\epsilon'\mu' < 0$ in which case (35) shows that the DDM always converges if $\epsilon' v_1' > 0$, even for a lossless material:

$$v_1'' \geqslant 0,\ \omega \in \mathbb{D}: \quad \epsilon'\mu' < 0,\ \epsilon' v_1' > 0 \Rightarrow E^{\ell} < E^{\ell-1} \tag{39}$$

These results can be extended to a 3D problem.

The global system reduced to the unknowns on interface S_1 is, as in Section 2.2, block-diagonal and writes $\mathbf{A}\underline{U} = \underline{F}$ with $\underline{u}_m = (b_{1m}, a_{1m}, b_{2m}, a_{2m})^t$, $\underline{f}_m = [0, 0, i^m, i^m(J_m'(k_0R_2) + \frac{v_1}{k_0}J_m(k_0R_2))/(\eta J_m'(kR_2) + \frac{v_1}{k_0}J_m(kR_2))]^t$ and

$$\mathbf{A}_m = \begin{pmatrix} \varphi_m & 1 & 0 & 0 \\ \psi_{1m}^+ & 1 & -\psi_{1m}^+ & -1 \\ \psi_{1m}^- & 1 & -\psi_{1m}^- & -1 \\ 0 & 0 & \psi_{2m} & 1 \end{pmatrix} \tag{40}$$

where

$$\psi_{2m} = \frac{\eta H_m'(kR_2) + \frac{v_1}{k_0}H_m(kR_2)}{\eta J_m'(kR_2) + \frac{v_1}{k_0}J_m(kR_2)}$$

comes from the ABC (33) on S_2, and $\det(\mathbf{A}_m) = (\psi_{1m}^+ - \psi_{1m}^-)(\varphi_m - \psi_{2m})$. (17) yields the TC on S_1 in (7) and (33) on S_2; $\mathbf{M}_m = \mathbf{A}_m$ except for the second row that writes $(\psi_{1m}^+/\omega, 1/\omega, 0, 0)$, and $\mathbf{N}_m = 0$ except for the second row that writes $(\psi_{1m}^+(1-\omega)/\omega, (1-\omega)/\omega, \psi_{1m}^+, 1)$. Then, the non-zero eigenvalues of $\mathbf{M}_m^{-1}\mathbf{N}_m$ are

$$\lambda_m = 1 + \omega(\lambda_m^0 - 1) \quad \lambda_m^0 = \frac{(\varphi_m - \psi_{1m}^-)(\psi_{1m}^+ - \psi_{2m})}{(\varphi_m - \psi_{1m}^+)(\psi_{1m}^- - \psi_{2m})} \tag{41}$$

We find the same ω dependency than in Després' algorithm [6], and (41) shows that relaxation is inefficient if $\lambda_m^0 \simeq 1$. Now, if we replace (7) by Després' algorithm – that results from a block Jacobi iterative solution of (14) –

$$\begin{aligned} T^+u_1^{\ell} &= (1-\omega)T^+u_1^{\ell-1} + \omega T^+u_2^{\ell-1} \\ T^-u_2^{\ell} &= (1-\omega)T^-u_2^{\ell-1} + \omega T^-u_1^{\ell-1} \end{aligned} \tag{42}$$

we get $\lambda_m = 1 + \omega(\sqrt{\lambda_m^0} - 1)$: again, as in Section 2.3, it shows that (42) converges less rapidly than (7).

3.2. Determination of the optimal v_1 for the model problem

We come back to the model problem in Section 2, but an exact TC defined by (26) is prescribed on S_3. This is realized if we set $R_3 = \infty$ and $v_{3m}^{\pm} = ik_0$, because of (30). To simplify, we consider the non-relaxed algorithm ($\omega = 1$): the λ_m are then given by (31). The issue is to determine the value v_{1opt} of v_1 that minimizes ρ as defined by (22). λ_m is numerically minimized by computing $\rho(v_1', v_1'')$, that necessitates to truncate the series in (2).

3.2.1. Determination of the truncation parameter in (2)

In (2), $2Q+1$ terms only are kept ($0 \leqslant |m| \leqslant Q$), and Q is such that the resulting error err_{RCS} on the Radar Cross Section (RCS), computed from S_2, is lower than a prescribed value ϵ_{RCS}:

$$\begin{aligned} &\sigma^{ex}(\theta) = b_0^{ex} + 2\sum_{m=0}^{\infty} i^m b_m^{ex}\cos m\theta \quad \sigma^{Q}(\theta) = b_0^{ex} + 2\sum_{m=0}^{Q} i^m b_m^{ex}\cos m\theta \\ &err_{RCS} = \frac{\|\sigma^{ex} - \sigma^{Q}\|}{\|\sigma^{ex}\|} \leqslant \epsilon_{RCS} \end{aligned} \tag{43}$$

b_m^{ex} is defined by the second identity in (4), $\|.\|$ is the L^2 norm and $RCS(\theta) = 10\log[4|\sigma(\theta)|^2/k_0]$. It is known [20,21] that:

$$Q = \xi k_0 R_2 \quad \xi > 1, \xi \simeq 1 \tag{44}$$

ξ is all the closer to one since k_0R_2 is large, and (44) is always satisfied in all what follows. Since the error is generally smaller on the far-field than on the near-field, the one achieved on $u(S_0)$ is also calculated:

$$err_u = \frac{\|u^{ex}(S_0) - u^{Q}(S_0)\|}{\|u^{ex}(S_0)\|} \tag{45}$$

$u^{ex}(S_0)$ is computed from (2) with $r = R_0$ and the coefficients a_m, b_m defined in (4); $u^{Q}(S_0)$ is computed from the truncated series. Unless otherwise mentioned, $\epsilon_{RCS} = 5 \cdot 10^{-3}$ in the following, that yields an error lower than 0.5 DB in $[0, 360^0]$ for the RCS, and $err_u < 10\%$ for all the numerical examples that are presented. We note that the accuracy obviously increases with Q: in a FEM, increasing Q is equivalent to a mesh refinement (see Section 6).

3.2.2. Numerical results

(37) is enforced in order to ensure unique solutions for the subproblems in each of the SDs, and $R_0 = 1m$ throughout this paper. We set

$$d_1 = R_1 - R_0 \quad d_2 = R_2 - R_0 \quad d_3 = R_3 - R_2$$

(here R_2 is fixed and $d_3 = \infty$). The results are shown for the less favorable TE polarization, because of the creeping (or evanescent) waves that are less attenuated in a lossless dielectric than in TM. For a lossy material, $H_m(x)$ ($J_m(x)$) decreases (respectively increases) exponentially with x and, in order to avoid accuracy problems, small losses only are considered. $\rho(m)$, as defined in (22), is plotted in Fig. 2 for various materials – only non-negative values of m are considered, on account of (3). The corresponding values of Q, v_{1opt}, ρ, err_{RCS} and err_u are reported in Table 1 where $\lambda = \lambda_0/\sqrt{|\epsilon\mu|}$ is the wavelength inside the material. We observe that ρ obtained with $v_1 = v_{1opt}$ is always smaller than ρ_{stand} calculated with the standard coefficient $v_1 = ik_0$, especially for the lossless dielectric $\epsilon = 2$, $\mu = 1$. Also, increasing Q (and, hence, the numerical accuracy) increases ρ and modifies the value of v_{1opt}, that is frequency dependent (not shown). As expected from (39), $\rho \ll 1$ when $v_1' > 0$ for $\epsilon = 2$ and $\mu = -1$ (we have verified that the same result is obtained for $\epsilon = -2$, $\mu = 1$ and $v_1' < 0$). Finally, we observe that ρ is smaller when losses are present (that implies $B''^{\ell} > 0$), according to (35).

3.3. Influence of the relaxation on the standard algorithm

Let us come back to the model problem defined in Section 2, and let $v_{1m}^{\pm}$, $v_{3m}^{\pm}$ satisfy (12); $\omega \in \mathbb{C}$ and $\rho(\omega', \omega'')$ is computed numerically. We have found that the value ω_{opt} of ω that minimizes ρ may be located outside of the disk $\mathbb{D}$ defined by (38)

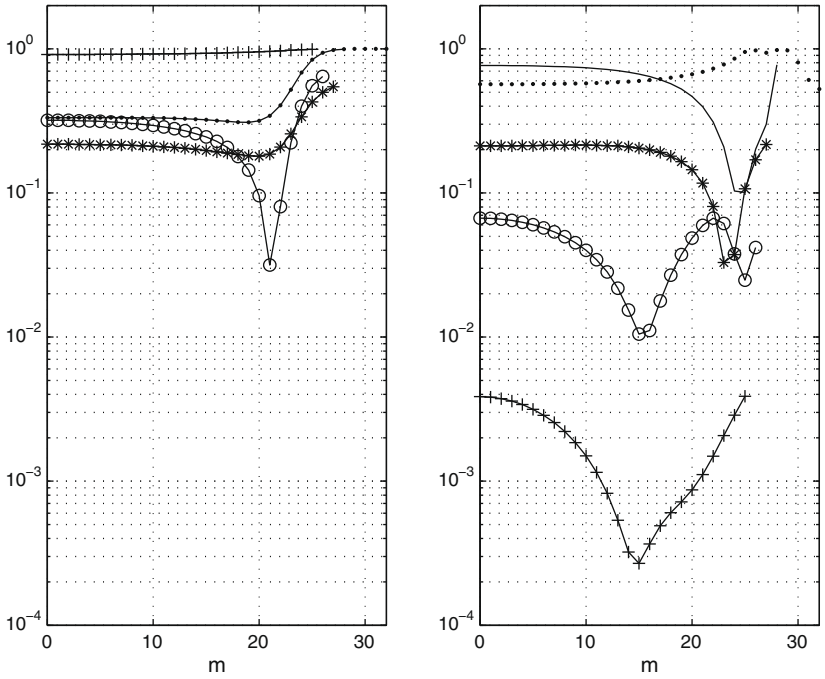

Fig. 2. $f = 1$ GHz. The values of R_1, R_2 are indicated in the caption of Table 1. Plots of $\rho_{stand}(m)$ (left: $v_{1m}^{+} = v_{1m}^{-} = ik_0$) and $\rho(m)$ (right: $v_{1m}^{+} = v_{1m}^{-} = v_{1opt}$) versus m. Solid line: $\epsilon = 2$, $\mu = 1$, $Q = 28$. Dotted line: $\epsilon = 2$, $\mu = 1$, $Q = 32$ (on the left, superimposed with the solid line for $m \leqslant 28$); $-*-$: $\epsilon = 2 - 0.1i$, $\mu = 1 - 0.1i$, $Q = 27$; $-+-$: $\epsilon = 2$, $\mu = -1$, $Q = 25$; $-\circ-$: $\epsilon = 5 - 0.1i$, $\mu = 2 - 0.1i$, $Q = 26$.

Table 1
$f = 1$ GHz. Four first rows: $R_1 = 1.05m$, $R_2 = 1.1m$, ($d_2 = 0.47\lambda$,$d_1 = d_2/2$). Last row ($\epsilon = 5 - 0.1i$, $\mu = 2 - 0.1i$): $R_1 = 1.02m$, $R_2 = 1.05m$ ($d_2 = 0.53\lambda$,$d_1 = d_2/2.5$). ρ_{stand} (ρ) is the radius of convergence obtained with $v_{1m}^{+} = v_{1m}^{-} = ik_0$ (respectively $v_{1m}^{+} = v_{1m}^{-} = v_{1opt}$).

Material	Q	v_{1opt}	ρ_{stand}	ρ	err_{RCS}	err_u
$\epsilon = 2$, $\mu = 1$	28	$-4.7 + 1.6i$	0.995	0.776	$1.7 \cdot 10^{-3}$	$3.9 \cdot 10^{-2}$
	32	$1.2 + 2.9i$	$1 - 10^{-5}$	0.98	$6.2 \cdot 10^{-7}$	$1.9 \cdot 10^{-4}$
$\epsilon = 2 - 0.1i$, $\mu = 1 - 0.1i$	27	$-2.3 + 8i$	0.545	0.217	$3.1 \cdot 10^{-3}$	$4.6 \cdot 10^{-2}$
$\epsilon = 2$, $\mu = -1$	25	$16.5 + 1.1i$	0.993	$3.9 \cdot 10^{-3}$	$4.3 \cdot 10^{-3}$	$2.8 \cdot 10^{-2}$
$\epsilon = 5 - 0.1i$, $\mu = 2 - 0.1i$	26	$-42 + 9.1i$	0.643	$6.7 \cdot 10^{-2}$	$1.8 \cdot 10^{-3}$	$2.6 \cdot 10^{-2}$

that guarantees $\rho < 1$, except for lossy materials for which $\omega_{opt} \simeq 1$, according to the analysis presented in Section 3.1. Since ω_{opt} is not known a priori, a possible solution is to generate ω_ℓ at random in [1/2,1] for each ℓ (with $\omega_1 = 1$). Numerical 2D and 3D results have demonstrated the efficiency of this procedure [6,15,16], that is easily justified for the model problem as follows. Let $\mathbf{P}_m^\ell$ denote the matrix $\mathbf{M}_m^{-1}\mathbf{N}_m$ where $\mathbf{M}_m$, $\mathbf{N}_m$ are defined in (18) and (19) with $\omega = \omega_\ell$. Then it can be shown analytically that the eigenvectors of $\mathbf{M}_m^{-1}\mathbf{N}_m$ that correspond to a non-zero eigenvalue λ_m^ℓ are ω_ℓ independent. As a result, the algorithm in (7) converges if $\rho = \max_m|\prod_{i=1}^{\ell}\rho_m^i| < 1$ ($\rho_m^i = \max|\lambda_m^i|$) that may yield a lower value of ρ than the one obtained with a fixed ω. However, we have observed that the relaxed standard algorithm (7) with (12) is much less efficient than the non-relaxed one with $v_1 = v_{1opt}$ as defined in Section 3.2.2.

4. Improved TCs

We show in Section 4.1 that choosing $v_m^+ \neq v_m^-$ and m independent enhances the performances of the TCs. Still higher performances are obtained in Section 4.2 with second order TCs, termed TC2, the numerical implementation of which in a FEM has been presented for standard H(rot) tetrahedral edge elements in [16]. We set $\omega_\ell = 1$ in all what follows.

4.1. $v_m^+ \neq v_m^-$ and m independent for the TCs on S_1 and S_3

4.1.1. Equivalence with the original problem without DDM, uniqueness and convergence

Here, $T^\pm$ in (7) writes, in TE:

$$S_1: \quad T^\pm = \frac{\partial_n}{\epsilon} \pm v_1^\pm \qquad S_3: \quad T^\pm = \partial_n \pm v_3^\pm \tag{46}$$

The TCs are well posed (i.e. the DDM is equivalent to the original problem) if, when $\ell \to \infty$, u^ℓ and $\partial_n u^\ell/\epsilon$ are continuous on S_1 and S_3 that, in view of (7) and (46), is realized if

$$i = 1,3: \quad v_i^+ + v_i^- \neq 0 \tag{47}$$

Regarding the uniqueness of the solutions in a SD, we consider, without loss of generality, the sourceless fields $(\underline{E},\underline{H})$ in the SD Ω bounded by S_1 and S_3. Consequently, we set $u_1^\ell = u_2^{\ell-1} = u_4^{\ell-1} = 0$ in (7). If we set $u = u_2^\ell$ for $R_1 \leqslant r \leqslant R_2$ and $u = u_3^\ell$ for $R_2 \leqslant r \leqslant R_3$, then (7) and (46) yield $\partial_n u/\epsilon = v_1^- u$ and $\partial_n u = -v_3^+ u$ as boundary conditions on S_1 and S_3, respectively, and the energy conservation writes:

$$A = k_0^2 \int_\Omega [\epsilon^*|\underline{E}|^2 - \mu|\underline{H}|^2] = \int_{S_3} u^* \partial_n u - \int_{S_1} u^* \frac{\partial_n u}{\epsilon} = -v_3^+ \int_{S_3} |u|^2 - v_1^- \int_{S_1} |u|^2 \tag{48}$$

Because $\Im(\epsilon), \Im(\mu) \leqslant 0, \Im(A) \geqslant 0$, and the fields are zero in Ω if

$$v_1^{-\prime\prime} \geqslant 0 \quad v_3^{+\prime\prime} \geqslant 0 \tag{49}$$

On the other hand, we cannot conclude for the convergence of the algorithm.

4.1.2. Exact TC on S_1

Interface S_1 is suppressed: two SDs remain on each side of S_3 (see Fig. 1), that amounts to consider the FEM-IE hybridization in [2] only. Such is the case if Maxwell's equations are solved exactly in the first SD (that includes all the materials) via one of the methods mentioned in Section 1. The λ_m are then given by (32) and are zero if $\varphi_m r_{\bar{m}}^- - r_{\bar{o}m}^- = 0$ or else, because of (21),

$$\psi_{3m}^- = \varphi'_m \Longleftrightarrow v_{3m}^- = k_0\eta\frac{J'_m(kR_1) - H'_m(kR_1)/\varphi'_m}{J_m(kR_1) - H_m(kR_1)/\varphi'_m}$$

$$\varphi'_m = \frac{\gamma_m - \gamma'_m + \varphi_m(\alpha_m\gamma'_m - \alpha'_m\gamma_m)}{\beta_m - \beta'_m + \varphi_m(\alpha_m\beta'_m - \alpha'_m\beta_m)}$$

For the particular case of free-space, (13) and (21) yield

$$\epsilon = \mu = 1 \Rightarrow r_{\bar{o}m}^\pm = \psi_{3m}^\pm r'_m; \quad r_{\bar{m}}^\pm = r'_m = \alpha'_m - \alpha_m$$

and (32) writes:

$$\lambda_m = \frac{\psi_{3m}^+(\psi_{3m}^- - \varphi_m)}{\psi_{3m}^-(\psi_{3m}^+ - \varphi_m)}$$

Hence $\lambda_m = 0$ if, e.g., $\psi_{3m}^- = \varphi_m$, that implies

$$v_{3m}^- = k_0\frac{J'_m(k_0R_3) - H'_m(k_0R_3)/\varphi_m}{J_m(k_0R_3) - H_m(k_0R_3)/\varphi_m}$$

Table 2
$f = 1$ GHz, exact TC on S_3 and TC (46) on S_1. $\rho_{stand} = \rho(v_1^+ = v_1^- = ik_0)$; $\rho_{opt} = \min_{v_1^{+'}, v_1^{+''}, v_1^{-'}, v_1^{-''}} \rho(v_1^{+'}, v_1^{+''}, v_1^{-'}, v_1^{-''}) = \rho(v_{1opt}^+, v_{1opt}^-)$; $\rho_{ap} = \rho(v_{1ap}^+, v_{1ap}^-)$; ρ is computed from (22) and (31). The numbers inside brackets indicate the formula that is employed to calculate $v_{1ap}^{\pm}$.

	$\epsilon = 2,\ \mu = 1,\ d_2 = 0.47\lambda;\ Q = 28$			$\epsilon = 2 - 0.1i,\ \mu = 1 - 0.1i,\ d_2 = 0.47\lambda,$ $d_1 = d_2/2$ (50); $Q = 27$	$\epsilon = 5 - 0.1i,\ \mu = 2 - 0.1i,\ d_2 = 0.53\lambda,$ $d_1 = d_2/2.5$ (50); $Q = 26$
	$d_1 = d_2/10$ (50)	$d_1 = d_2/2$ (50)	$d_1 = d_2/1.4$ (51)		
v_{1opt}^+	$-3.7 + 13i$	$2.5 - 0.2i$	$5.2 + 0.23i$	$0.45 + 10.4i$	$-3.2 + 11.8i$
v_{1ap}^+	$-3.4 + 13.2i$	$0.15 + 8.9i$	$5.4 + 0.067i$	$0.8 + 10.3i$	$-4.4 + 13.5i$
v_{1opt}^-	$-0.55 + 0.012i$	$-15.7 + 3.4i$	$-15 + 35i$	$-5.8 + 4.7i$	$-33.7 + 6.3i$
v_{1ap}^-	-0.51	-3.6	$20.96i = ik_0$	$-4.7 + 4.1i$	$-32 + 5.6i$
ρ_{stand}	0.996	0.995	0.994	0.54	0.64
ρ_{opt}	0.076	0.48	0.43	0.08	0.017
ρ_{ap}	0.087	0.71	0.44	0.12	0.033

If $k_0R_3 \simeq k_0R_0$ then, because of the definition of φ_m in (5), we get $v_{3m}^- \simeq 0$ in TE and $v_{3m}^- \gg k_0$ in TM, i.e. a quasi-exact TC since v_{3m}^- is almost m independent.

4.1.3. Determination of the optimal values of v_1^+, v_1^- with an exact TC on S_3

An exact TC is prescribed on S_3 (e.g., v_3^+, v_3^- satisfy (12) and $R_3 \gg R_2$) in which case the λ_m are given by (31). Minimizing analytically λ_m with respect to the real and imaginary parts of v_1^+, v_1^- is not straightforward. For this reason, we adopt an heuristic approach, justified in Appendix B, that gives the following approximate values v_{1ap}^-, v_{1ap}^+ for v_1^-, v_1^+ that minimize ρ – $D(x)$ is defined by (82) –:

$$\forall x \in [0, Q],\ D(x) \neq 0: \quad v_{1ap}^- = v_{1Q}^- = k_0\eta \frac{J_Q'(kR_1)\varphi_Q - H_Q'(kR_1)}{J_Q(kR_1)\varphi_Q - H_Q(kR_1)}$$
$$v_{1ap}^+ = -\frac{k_0\eta}{Q} \sum_{m=0}^{Q} \frac{H_m'(kR_1) - J_m'(kR_1)r_m^\infty}{H_m(kR_1) - J_m(kR_1)r_m^\infty} \tag{50}$$

$$\exists x \in [0, Q] \setminus D(x) = 0: \quad v_{1ap}^- = ik_0$$
$$v_{1ap}^+ = v_{1Q}^+ = -k_0\eta \frac{H_Q'(kR_1) - J_Q'(kR_1)r_Q^\infty}{H_Q(kR_1) - J_Q(kR_1)r_Q^\infty} \tag{51}$$

In the first case (50), the numerical results show that the value of v_{1ap}^- governs ρ (v_1^- acts on the evanescent modes $m \simeq Q$), whereas it is the opposite for (51). Note (see Appendix B) that $D(x)$ is likely to be different from zero (i) if there are losses and (ii) for a lossless material, if the location of S_1 is such that (83) is not satisfied. As in the previous section, when $|k|R_1 \simeq |k|R_0$, (50) implies $v_1^- \simeq 0$ in TE and $v_1^- \gg k_0$ in TM that guarantee a fast convergence. Finally, from (5) and because of the definition $H_m(x) = J_m(x) - iY_m(x)$, we note that (50) implies $v_{1ap}^- \in \mathbb{R}$ when $\epsilon, \mu \in \mathbb{R}$ and, hence, (49) is satisfied.

We have numerically computed the values, v_{1opt}^+ and v_{1opt}^-, of v_1^+ and v_1^- that minimize $\rho(v_1^{+'}, v_1^{+''}, v_1^{-'}, v_1^{-''})$. The corresponding results are presented in Table 2 and Fig. 3 for $f = 1$ GHz, $R_3 = 100m$ and in TE polarization (the less favorable, because of the creeping waves) that lead to the following conclusions. (i) These TCs actually perform better than those with $v_1^+ = v_1^-$ in the same configurations (compare with Table 1 and Fig. 2). (ii) (50) and (51) constitute reasonable approximations of $v_{1opt}^{\pm}$ – that implies $\rho_{ap} \simeq \rho_{opt}$ (these quantities are defined in the caption of Table 2) – except, for a lossless material, in the transition zone between $D(x) \neq 0$ and $D(x) = 0$ that, because of (83), corresponds here to $d_1 = \lambda/4$. (iii) We have verified that v_1^- (v_1^+) governs the convergence when R_1 is close to R_0 (respectively R_2). This means, for example, that when $kR_1 \simeq kR_0$, ρ_{opt} is almost independent of v_1^+ as long as $v_1^- \simeq 0$. The plots of ρ_{ap} in Fig. 3 clearly show the action of the TC on the evanescent waves: $\rho_{ap}(Q) \ll 1$.

4.1.4. Approximate TCs on S_1 and S_3

Both TCs on S_1 and S_3 are now defined by (46), and the resulting λ_m by (25). If (50) and (51) constitute good approximations of the exact TC on S_1, then the λ_m are approximately given by (32) that are zero if $\psi_{3m}^+ = 0$ and hence, on account of (11), if $v_{3m}^+ = -k_0H_m'(k_0R_3)/H_m(k_0R_3)$. Numerical results show that the following values of the coefficients, that do not depend on m, yield satisfying results:

$$v_{3ap}^+ = -\frac{k_0}{Q} \sum_{m=0}^{Q} \frac{H_m'(k_0R_3)}{H_m(k_0R_3)} \quad v_{3ap}^- = ik_0 \tag{52}$$

Since[1] $v_{3ap}^{\pm'} > 0$, v_{3ap}^+ and v_{3ap}^- satisfy (49). When $k_0R_3 > k_0R_2 + O[k_0R_2)^{1/3}]$, i.e. when S_3 is outside of the evanescent region, we easily get in Appendix C the following "geometrical" approximation for v_{3ap}^+:

[1] See Appendix C; also, $v_{3ap}^{+'} > 0$, because $\Re\left[\frac{H_m'(k_0R_3)}{H_m(k_0R_3)}\right] < 0$ [19].

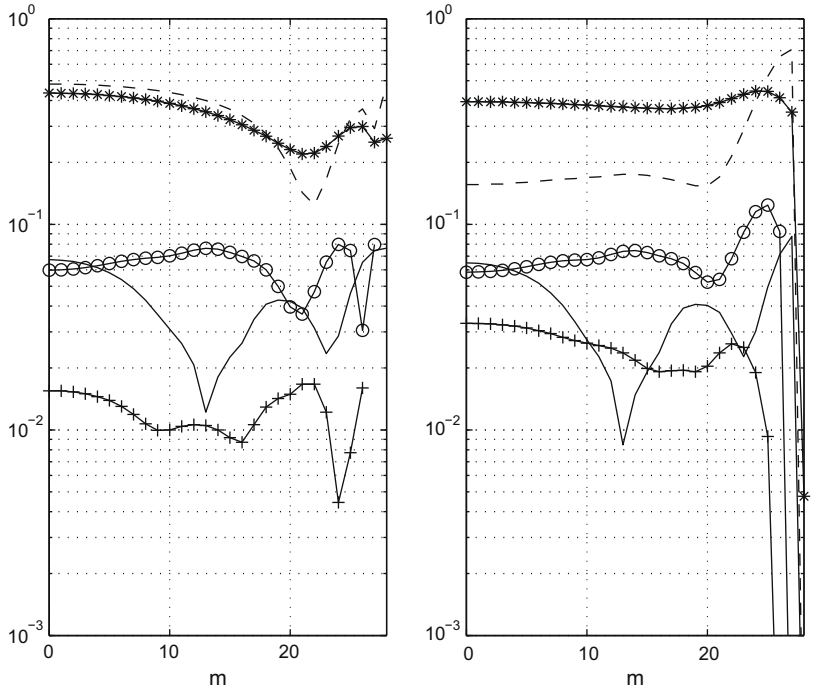

Fig. 3. $f = 1$ GHz, exact TC on S_3 and TC (46) on S_1. Same parameters than in Table 2; ρ is computed from (22) and (31). Left: $\rho_{opt}(m) = \rho(v^+_{1opt}, v^-_{1opt})$ versus m. Right: $\rho_{ap}(m) = \rho(v^+_{1ap}, v^-_{1ap})$ versus m. Solid line: $\epsilon = 2$, $\mu = 1$, $d_1 = d_2/10$. Dashed line: $\epsilon = 2$, $\mu = 1$, $d_1 = d_2/2$; $-*-$: $\epsilon = 2$, $\mu = 1$, $d_1 = d_2/1.4$; $-\circ-$: $\epsilon = 2 - 0.1i$, $\mu = 1 - 0.1i$, $d_1 = d_2/2$; $-+-$: $\epsilon = 5 - 0.1i$, $\mu = 2 - 0.1i$, $d_1 = d_2/2.5$.

$$v^{+'}_{3ap} \simeq \frac{1}{2R_2} arcth \sin\zeta > 0 \quad v^{+''}_{3ap} \simeq \frac{k_0}{2}\left[\cos\zeta + \frac{\zeta}{\sin\zeta}\right] > 0 \quad \zeta = arcsin\frac{R_2}{R_3} \tag{53}$$

In high frequency electromagnetics, ζ is the angle of incidence on S_3 of a ray tangent to S_2 (see Fig. 1): as a consequence, it is the maximum angle of incidence on S_3 of a ray reflected by S_2, or creeping on S_2. Also, we note that (52) and (53) yield the expected value when R_3 is large, i.e., $lim_{R_3\to\infty} v^+_{3ap} = ik_0$. Finally, we may use this value of v^+_{3ap} to get an efficient ABC on S_3 that writes – see (33) – $(\partial_n + v^+_{3ap})u_4 = (\partial_n + v^+_{3ap})u^{inc}$. Actually, $\psi^+_{3m} = 0$ is the definition of an exact ABC on S_3, because of (29).

Figs. 4–6 display the performances of these new TCs (only the polarizations that yield the worst results are shown). As mentioned before, we observe that they are less efficient for a lossless material and for the values of d_1/λ given by (83) that yield $D(m) \simeq 0$ – except when $R_1 \simeq R_0$ in TM. Figs. 7 and 8 show that approximation (53) is reasonable. Also, $v^{+''}_{1ap} > 0$ (not shown for $\epsilon = 5$, $\mu = 2$), that entails unique solutions in the first SD bounded by S_0 and S_1 (see Section 4.1.1) – uniqueness of the solutions in the second SD is guaranteed since $v^{-''}_{1ap} \geqslant 0$. Let us mention that numerical results show that implementing the TC (46) on S_3 only is not efficient.

4.2. Second order TCs (TC2s) on S_1 and S_3

The TC2s involve second order tangential derivatives of the fields on the interfaces. The operators $T^{\pm}$ defined in (7) and implemented in 2D in [15] write, on interface S_3 (e.g.),

$$\begin{aligned} &T^{\pm} = \partial_n \pm (v_{31} + v_{32}\partial_l^2) \\ &v_{31} = ik_0\left[\frac{1 - \frac{3i}{2k_0R_3} - \frac{3}{8(k_0R_3)^2}}{1 - \frac{i}{k_0R_3}}\right] \quad v_{32} = \frac{i}{2k_0\left(1 - \frac{i}{k_0R_3}\right)} \end{aligned} \tag{54}$$

where l designate the curvilinear abscissa and ∂_l the partial derivative with respect to l. These TC2s, as well as their 3D counterpart [16], yield good results in free-space. However, for this model problem, we have observed that they are inefficient in a lossless material.

We set, as in Section 4.1, $v^+_{31} \neq v^-_{31}$, $v^+_{32} \neq v^-_{32}$ and, for S_1, $v^+_{11} \neq v^-_{11}$, $v^+_{12} \neq v^-_{12}$. Then operators $T^{\pm}$ write:

$$S_1: \quad T^{\pm} = \frac{\partial_n}{\epsilon} \pm (v^{\pm}_{11} + v^{\pm}_{12}\partial_l^2) \qquad S_3: \quad T^{\pm} = \partial_n \pm (v^{\pm}_{31} + v^{\pm}_{32}\partial_l^2) \tag{55}$$

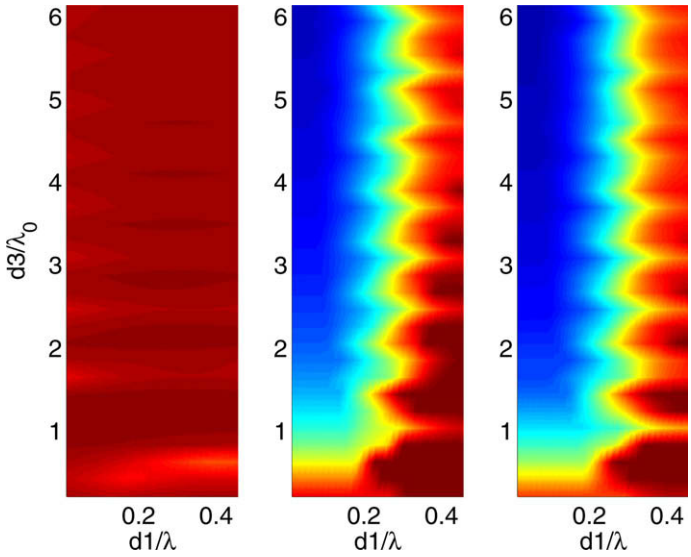

Fig. 4. $\epsilon = 2$, $\mu = 1$, $f = 1$ GHz, $R_2 = 1.1m$ ($d_2 = 0.47\lambda$), TM. $\min(1,\rho)$ versus d_1/λ and d_3/λ_0. Left: standard TC on S_1 and S_3 ($v^+_{1m} = v^-_{1m} = v^+_{3m} = v^-_{3m} = ik_0$). Middle: TC (46) on S_1 with $v^\pm_{1m} = v^\pm_{1ap}$ computed from (50) or (51), and standard TC on S_3 ($v^+_{3m} = v^-_{3m} = ik_0$). Right: TC (46) on S_1 and S_3 with $v^\pm_{1m} = v^\pm_{1ap}$ computed from (50) or (51), and $v^\pm_{3m} = v^\pm_{3ap}$ computed from (52). Dark red: $\min(1,\rho) = 1$; Dark blue: $\min(1,\rho) = 0$. (For interpretation of the references to colour in this figure legend, the reader is referred to the web version of this article.)

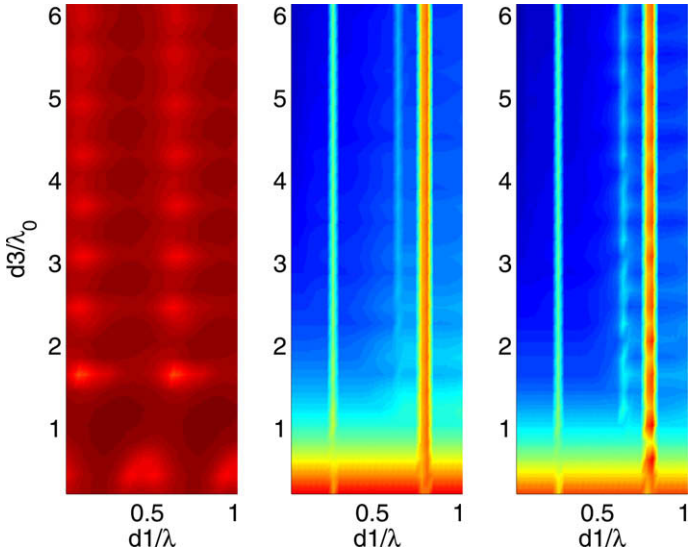

Fig. 5. $\epsilon = 5$, $\mu = 2$, $f = 1$ GHz, $R_2 = 1.1m$ ($d_2 = 1.06\lambda$), TE. Same caption as in Fig. 4.

For the model problem, because $\partial_l = \partial_\theta/R$ on a circle of radius R, this amounts to set in (11):

$$v^\pm_{im} = v^\pm_{i1} - \frac{m^2 v^\pm_{i2}}{R_i^2} \quad i = 1,3 \tag{56}$$

Coefficients $v^\pm_{i2}$ act on evanescent waves, as it can be observed for the TC2 on S_3 defined by (54): if $k_0 R_3 \gg 1$, then $v^\pm_{3m} \simeq ik_0[1 - \frac{m^2}{2(k_0R_3)^2}]$, the difference of which with ik_0 is maximum for $m = Q \simeq k_0 R_2$.

Regarding the uniqueness of the solutions in each SD, (48) yields, after integration by parts,

$$A = k_0^2 \int_\Omega [\epsilon^* |\underline{E}|^2 - \mu |\underline{H}|^2] = -v^+_{31} \int_{S_3} |u|^2 - v^-_{11} \int_{S_1} |u|^2 + v^+_{32} \int_{S_3} |\partial_l u|^2 + v^-_{12} \int_{S_1} |\partial_l u|^2 \tag{57}$$

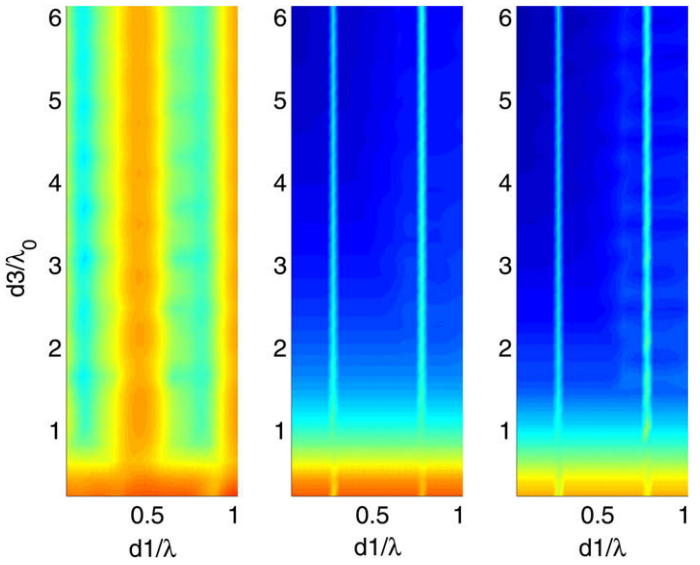

Fig. 6. $\epsilon = 5 - 0.1i$, $\mu = 2 - 0.1i$, $f = 1$ GHz, $R_2 = 1.1m$ ($d_2 = 1.06\lambda$), TE. Same caption as in Fig. 4.

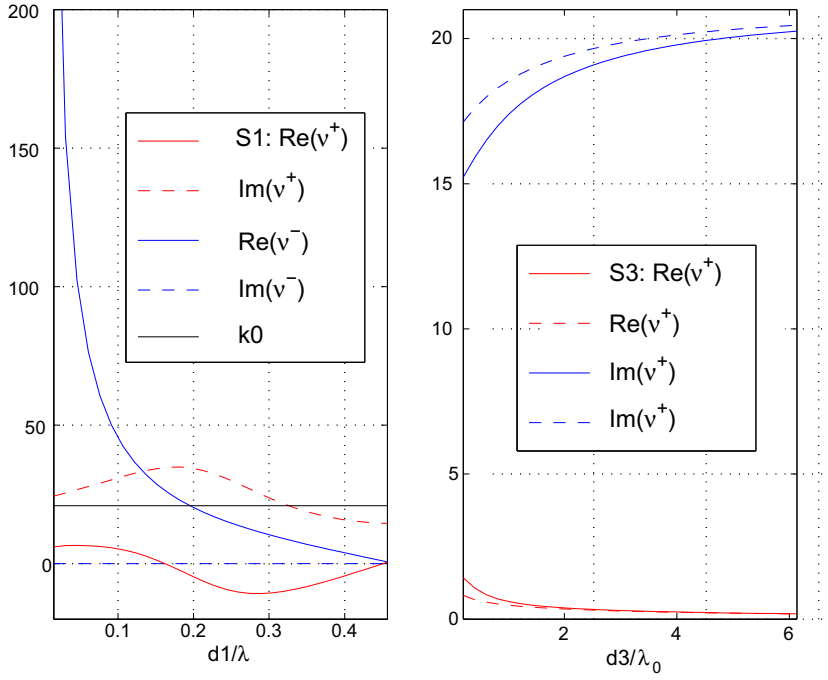

Fig. 7. Same caption as in Fig. 4. Left: TC on S_1, $v^{\pm}_{1ap}$ (50) and (51) versus d_1/λ. Right: TC on S_3, $v^{\pm}_{3ap}$ (52) (solid lines) and its geometrical approximation (53) (dashed lines) versus d_3/λ_0.

and, because $\Im(A) \geqslant 0$, uniqueness is guaranteed if:

$$v_{11}^{-\prime\prime} \geqslant 0 \quad v_{31}^{+\prime\prime} \geqslant 0 \quad v_{12}^{-\prime\prime} \leqslant 0 \quad v_{32}^{+\prime\prime} \leqslant 0 \tag{58}$$

We cannot conclude for the convergence of the algorithm.

We proceed as in Section 4.1.3 (see also Appendix B) to determine the approximate values of the parameters $v^{\pm}_{i1}, v^{\pm}_{i2}$ $(i = 1, 3)$ that minimize ρ. For the TC2 on S_1, we consider the case where the TC on S_3 is exact, i.e. we attempt to minimize λ_m defined by (31). To this end, we set $\psi^{-}_{1m} = \varphi_m$ and $\psi^{+}_{1m} = r^{\infty}_m$ for $m = Q$, in other words, we enforce the TC2 to act mainly on the evanescent waves. Then (11) and (56) imply:

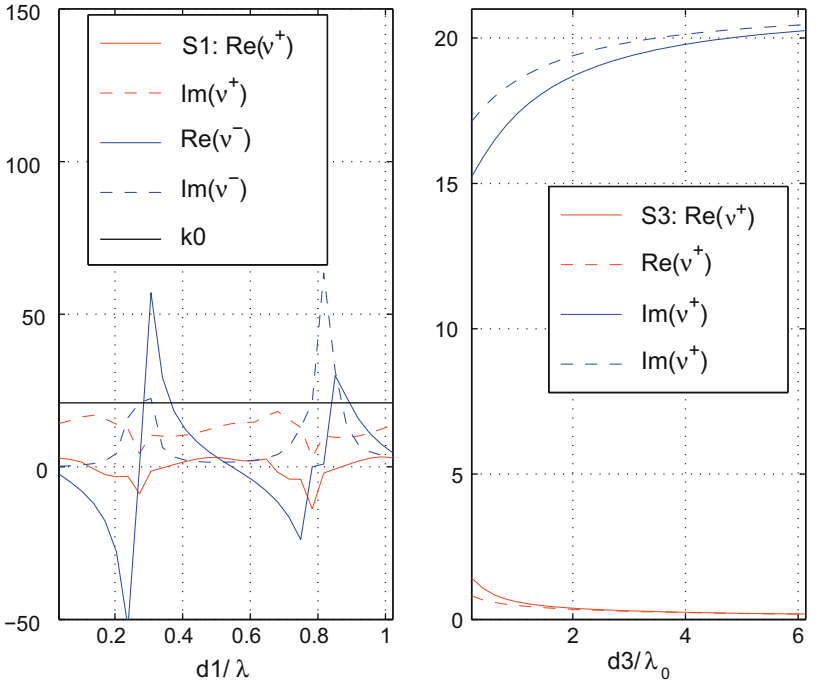

Fig. 8. Same caption as in Fig. 6. Left: TC on S_1, $v^{\pm}_{1ap}$ (50) and (51) versus d_1/λ. Right: TC on S_3, $v^{\pm}_{3ap}$ (52) (solid lines) and its geometrical approximation (53) (dashed lines) versus d_3/λ_0.

$$
\begin{aligned}
v^{+}_{12ap} &= \frac{R_1^2}{Q^2}\left[k_0\eta\frac{H'_Q(kR_1)-J'_Q(kR_1)r^{\infty}_Q}{H_Q(kR_1)-J_Q(kR_1)r^{\infty}_Q}+v^{+}_{11ap}\right]\\
v^{-}_{12ap} &= -\frac{R_1^2}{Q^2}\left[k_0\eta\frac{J'_Q(kR_1)\varphi_Q-H'_Q(kR_1)}{J_Q(kR_1)\varphi_Q-H_Q(kR_1)}+v^{-}_{11ap}\right]\\
v^{\pm}_{11ap} &= v^{\pm}_{1ap}
\end{aligned}
\tag{59}
$$

$v^{\pm}_{1ap}$ are defined[2] by (50). For the TC2 on S_3, we consider the case where the TC on S_1 is exact, i.e. we attempt to minimize λ_m defined by (32). We set $\psi^{+}_{3m}=0$ for $m=Q$, i.e. we choose $v^{+}_{32}=v^{+}_{32ap}$ such that the TC2 acts essentially on the evanescent waves. Because of (11) and (56), we get

$$
v^{\pm}_{31ap}=v^{\pm}_{3ap};\quad v^{+}_{32ap}=\frac{R_3^2}{Q^2}\left[k_0\frac{H'_Q(k_0R_3)}{H_Q(k_0R_3)}+v^{+}_{31ap}\right];\quad v^{-}_{32ap}=\frac{i}{2k_0(1-\frac{i}{k_0R_3})}
\tag{60}
$$

where $v^{\pm}_{3ap}$ are defined by (52). We have observed numerically that the performance of the TC2 on S_3 depends but slightly on v^{-}_{32ap} that is consequently set to the value defined in (54). If Debye's approximation (85) is employed to evaluate v^{+}_{32ap}, then we get $v^{+''}_{32ap}>0$ and the sufficient uniqueness condition (58) is not satisfied in any SD – we obtain the same result for v_{32} defined by (54). Actually, (60), (86) and (53) imply, with $Q\simeq k_0R_2$:

$$
v^{+}_{32ap}\simeq\frac{1}{2k_0\sin^2\zeta}\left[\frac{1}{k_0R_2}arcth\sin\zeta-\frac{\sin\zeta}{\cos^2\zeta}+i\left(\frac{\zeta}{\sin\zeta}-\cos\zeta\right)\right]
$$

We deduce from this expression that $1/(3k_0)\leqslant v^{+''}_{32ap}\leqslant\pi/(4k_0)$; since $v^{+''}_{32ap}(\zeta)$ is an increasing function of ζ in $[0,\pi/2]$, it is strictly positive. As in Section 4.1.4, we note that these values of $v^{+}_{31ap}, v^{+}_{32ap}$ define a more performing second order ABC on S_3 than the one in (54).

Numerical results (not shown) show that the new TC2, implemented on S_3 only, enhances the efficiency of the TC on S_1 defined in Section 4.1.4. Figs. 9–11 demonstrate the superior performances of the TC2 defined by (55), (59), (60) that are implemented either on S_1 only, or on both S_1 and S_3 (compare to Figs. 4–6).

[2] Numerical results show that satisfying results are obtained if $v^{\pm}_{11ap}$ is computed from (50) even when $D(x)$ has a zero in $[0,Q]$.

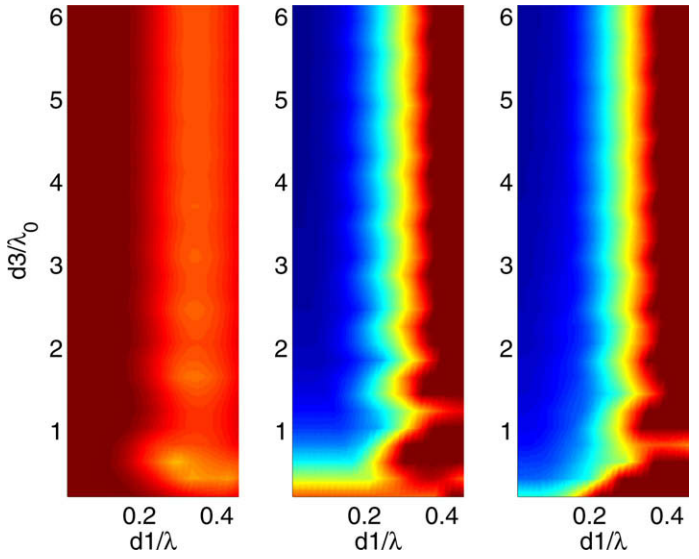

Fig. 9. $\epsilon = 2$, $\mu = 1$, $f = 1$ GHz, $R_2 = 1.1m$ ($d_2 = 0.47\lambda$), TM. $\min(1,\rho)$ versus d_1/λ and d_3/λ_0. Left: standard TC2 (54) on S_1 and S_3. Middle: TC2 (55) and (59) on S_1, and standard TC2 (54) on S_3. Right: TC2 (55) on S_1 and S_3, and (59) on S_1, (60) on S_3.

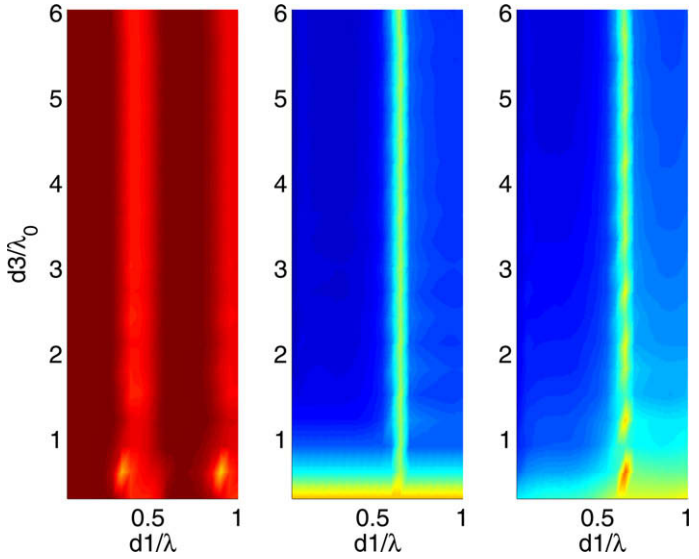

Fig. 10. $\epsilon = 5$, $\mu = 2$, $f = 1$ GHz, $R_2 = 1.1m$ ($d_2 = 1.06\lambda$), TE. Same caption as in Fig. 9.

5. An additional interface

An additional interface S_{12} of radius R_{12} is located inside the material between S_1 and S_2 ($R_1 < R_{12} < R_2$). Following along the same lines than in Section 2.2, we get (14) with $\underline{u}_m = (b_{1m}, a_{1m}, b_{21m}, a_{21m}, b_{22m}, a_{22m}, b_{3m}, a_{3m}, b_{4m})^t$ and $\underline{f}_m = (0,0,0,0,0,0,0,0,i^m,i^m)^t$

$$
\begin{aligned}
S_1: \quad & a^{\ell}_{1m} + \psi^{+}_{1m} b^{\ell}_{1m} = a^{\ell-1}_{21m} + \psi^{+}_{1m} b^{\ell-1}_{21m} \\
& a^{\ell}_{21m} + \psi^{-}_{1m} b^{\ell}_{21m} = a^{\ell}_{1m} + \psi^{-}_{1m} b^{\ell}_{1m} \\
S_{12}: \quad & a^{\ell}_{21m} + \psi^{+}_{12m} b^{\ell}_{21m} = a^{\ell-1}_{22m} + \psi^{+}_{12m} b^{\ell-1}_{22m} \\
& a^{\ell}_{22m} + \psi^{-}_{12m} b^{\ell}_{22m} = a^{\ell}_{21m} + \psi^{-}_{12m} b^{\ell}_{21m} \\
& \psi^{\pm}_{12m} = \frac{\eta H'_m(kR_{12}) \pm \frac{v^{\pm}_{12m}}{k_0} H_m(kR_{12})}{\eta J'_m(kR_{12}) \pm \frac{v^{\pm}_{12m}}{k_0} J_m(kR_{12})}
\end{aligned}
\tag{61}
$$

The TC on S_3 in (10) is unchanged, as well as (13). This yields

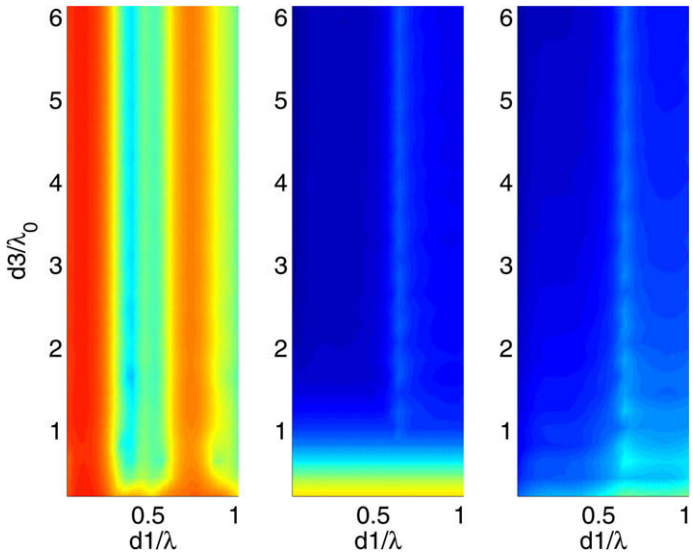

Fig. 11. $\epsilon = 5 - i0.1$, $\mu = 2 - i0.1$, $f = 1$ GHz, $R_2 = 1.1m$ ($d_2 = 1.06\lambda$), TE. Same caption as in Fig. 9.

$$\mathbf{A}_m = \begin{pmatrix} \varphi_m & 1 & 0 & 0 & 0 & 0 & 0 & 0 & 0 \\ \psi^+_{1m} & 1 & -\psi^+_{1m} & -1 & 0 & 0 & 0 & 0 & 0 \\ \psi^-_{1m} & 1 & -\psi^-_{1m} & -1 & 0 & 0 & 0 & 0 & 0 \\ 0 & 0 & \psi^+_{12m} & 1 & -\psi^+_{12m} & -1 & 0 & 0 & 0 \\ 0 & 0 & \psi^-_{12m} & 1 & -\psi^-_{12m} & -1 & 0 & 0 & 0 \\ 0 & 0 & 0 & 0 & 1 & \alpha_m & -\gamma_m & -\beta_m & 0 \\ 0 & 0 & 0 & 0 & 1 & \alpha'_m & -\gamma'_m & -\beta'_m & 0 \\ 0 & 0 & 0 & 0 & 0 & 0 & \psi^+_{3m} & 1 & -\psi^+_{3m} \\ 0 & 0 & 0 & 0 & 0 & 0 & \psi^-_{3m} & 1 & -\psi^-_{3m} \end{pmatrix} \tag{62}$$

for matrix $\mathbf{A}_m$ in (14), and

$$\mathbf{M}_m = \begin{pmatrix} \varphi_m & 1 & 0 & 0 & 0 & 0 & 0 & 0 & 0 \\ \psi^+_{1m} & 1 & 0 & 0 & 0 & 0 & 0 & 0 & 0 \\ \psi^-_{1m} & 1 & -\psi^-_{1m} & -1 & 0 & 0 & 0 & 0 & 0 \\ 0 & 0 & \psi^+_{12m} & 1 & 0 & 0 & 0 & 0 & 0 \\ 0 & 0 & \psi^-_{12m} & 1 & -\psi^-_{12m} & -1 & 0 & 0 & 0 \\ 0 & 0 & 0 & 0 & 1 & \alpha_m & -\gamma_m & -\beta_m & 0 \\ 0 & 0 & 0 & 0 & 1 & \alpha'_m & -\gamma'_m & -\beta'_m & 0 \\ 0 & 0 & 0 & 0 & 0 & 0 & \psi^+_{3m} & 1 & 0 \\ 0 & 0 & 0 & 0 & 0 & 0 & \psi^-_{3m} & 1 & -\psi^-_{3m} \end{pmatrix}$$

$$\mathbf{N}_m = \begin{pmatrix} 0 & 0 & 0 & 0 & 0 & 0 & 0 & 0 & 0 \\ 0 & 0 & \psi^+_{1m} & 1 & 0 & 0 & 0 & 0 & 0 \\ 0 & 0 & 0 & 0 & 0 & 0 & 0 & 0 & 0 \\ 0 & 0 & 0 & 0 & \psi^+_{12m} & 1 & 0 & 0 & 0 \\ 0 & 0 & 0 & 0 & 0 & 0 & 0 & 0 & 0 \\ 0 & 0 & 0 & 0 & 0 & 0 & 0 & 0 & 0 \\ 0 & 0 & 0 & 0 & 0 & 0 & 0 & 0 & 0 \\ 0 & 0 & 0 & 0 & 0 & 0 & 0 & 0 & \psi^+_{3m} \\ 0 & 0 & 0 & 0 & 0 & 0 & 0 & 0 & 0 \end{pmatrix}$$

for the (unrelaxed) block Gauss–Seidel decomposition (17) of $\mathbf{A}_m$. The objective here is to investigate the influence of this additional interface on the convergence of the algorithm defined by (17). To facilitate the closed-form derivation of the eigenvalues λ_{12m} of $\mathbf{M}_m^{-1}\mathbf{N}_m$, we set $\psi^+_{3m} = 0$, viz. an exact TC is prescribed on S_3. Then, the non-zero λ_{12m} write:

$$\begin{aligned}
&\lambda_{12m} = (-b \pm \sqrt{b^2 - 4c})/2 \\
&b = \frac{1}{\psi_{1m}^- - \psi_{12m}^+}\left\{\frac{(\varphi_m - \psi_{1m}^-)(\psi_{12m}^+ - \psi_{1m}^+)}{\varphi_m - \psi_{1m}^+} + \frac{(\psi_{12m}^+ - r_m^\infty)(\psi_{12m}^- - \psi_{1m}^-)}{\psi_{12m}^- - r_m^\infty}\right\} \\
&c = \frac{(\psi_{12m}^+ - r_m^\infty)(\varphi_m - \psi_{1m}^-)(\psi_{12m}^- - \psi_{1m}^+)}{(\varphi_m - \psi_{1m}^+)(\psi_{12m}^- - r_m^\infty)(\psi_{12m}^+ - \psi_{1m}^-)}
\end{aligned} \tag{63}$$

$\rho_{12} = \max_m(\max|\lambda_{12m}|)$ designates the corresponding radius of convergence of (17), as opposed to ρ in (22) obtained without the S_{12} interface. The problem is well posed if $\det(\mathbf{A}_m) \neq 0$ that, in view of (62), implies $\psi_{12m}^+ \neq \psi_{12m}^-$. Because of (31), the exact TC on S_1 is obtained if $\psi_{1m}^- = \varphi_m$ or $\psi_{1m}^+ = r_m^\infty$, and (63) shows that $\rho_{12} = 0$ if $\psi_{12m}^+ = r_m^\infty$ or $\psi_{12m}^- = \varphi_m$ in the former case, and $\psi_{12m}^+ = r_m^\infty$ in the latter. It is noteworthy that $\psi_{12m}^\pm = \psi_{1m}^\pm$ yields $\lambda_{12m} = \sqrt{\lambda_m}$ where λ_m is defined by (31), so that

$$\psi_{3m}^+ = 0, \quad \psi_{12m}^\pm = \psi_{1m}^\pm \Rightarrow \rho_{12} = \sqrt{\rho} \tag{64}$$

This identity illustrates the well-known fact that the convergence of the DDM algorithm is slowed down when an additional interface is introduced.

Numerical experiments performed with $v_{1m}^\pm = v_{1ap}^\pm$ as defined in (50) and (51) have shown that moderate values of ρ_{12} are achieved for an arbitrary R_{12} if $v_{12m}^\pm = v_{12ap}^\pm$:

$$\begin{aligned}
v_{12ap}^- &= v_{12Q}^- = k_0\eta\frac{J_Q'(kR_{12})\varphi_Q - H_Q'(kR_{12})}{J_Q(kR_{12})\varphi_Q - H_Q(kR_{12})} \\
v_{12ap}^+ &= -\frac{k_0\eta}{Q}\sum_{m=0}^{Q}\frac{H_m'(kR_{12}) - J_m'(kR_{12})r_m^\infty}{H_m(kR_{12}) - J_m(kR_{12})r_m^\infty}
\end{aligned} \tag{65}$$

These coefficients, that do not depend on m, enforce $\psi_{12Q}^- = \varphi_Q$ and the averaged value on m of ψ_{12m}^+ equal to the one of r_m^∞ (see definition (61) of $\psi_{12m}^\pm$). We observe on Figs. 12 and 13 (the worst results are obtained in TE) that (64) is approximately verified. Also, $v_{1ap}^{+''}, v_{12ap}^{-''} \geqslant 0$: (49) is satisfied and uniqueness of the solutions is guaranteed in each SD.

6. Elliptical PEC cylinder with two subdomains

In this section, we consider the scattering problem by an elliptical PEC cylinder of surface S_0 embedded in free-space and illuminated by the plane wave e^{ik_0x}. a_0 (b_0) denotes the half major (respectively minor) axis along x (respectively y) of S_0 and $c = \sqrt{a_0^2 - b_0^2}$ is the half interfocal distance. An elliptical interface S_1 of half major and minor axes $a_1 \geqslant a_0$ and $b_1 \geqslant b_0$ partitions the computational domain into two concentric subdomains Ω_1 and Ω_2 with $\partial\Omega_1 = S_0 \cup S_1$. S_0 and S_1 have the same foci, so that:

$$b_1 = \sqrt{a_1^2 - c^2} \tag{66}$$

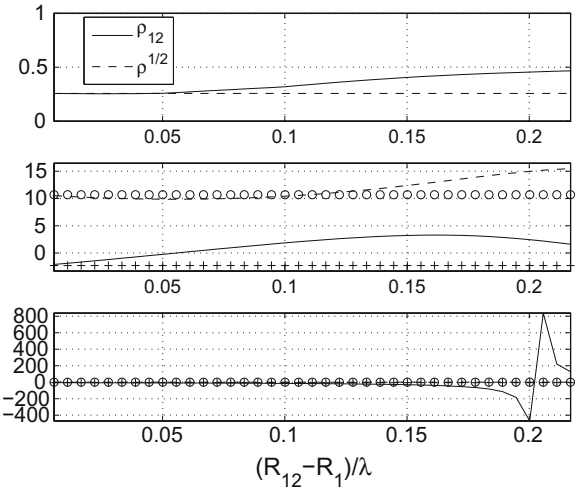

Fig. 12. $\epsilon = 2$, $\mu = 1$, $f = 1$ GHz, $R_2 = 1.1m$ ($d_2 = 0.47\lambda$), $R_1 = R_0 + (R_2 - R_0)/3$, TE. Top: ρ_{12} and $\rho^{1/2}$ versus $(R_{12} - R_1)/\lambda$. Middle: $v_{1ap}^{+'}$ (+), $v_{1ap}^{+''}$ (○) computed from (50) and $v_{12ap}^{+'}$ (solid line), $v_{12ap}^{+''}$ (dashed line) computed from (65), versus $(R_{12} - R_1)/\lambda$. Bottom: $v_{1ap}^{-'}$ (+), $v_{1ap}^{-''}$ (○) computed from (50) and $v_{12ap}^{-'}$ (solid line), $v_{12ap}^{-''}$ (dashed line) computed from (65), versus $(R_{12} - R_1)/\lambda$.

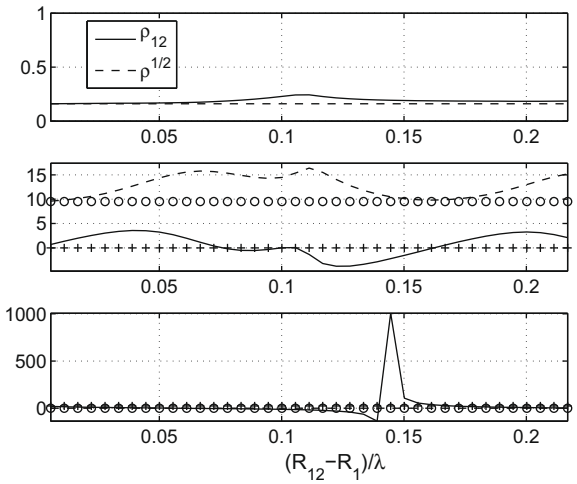

Fig. 13. $\epsilon = 5$, $\mu = 2$, $f = 1$ GHz, $R_2 = 1.1m$ ($d_2 = 1.06\lambda$), $R_1 = R_0 + (R_2 - R_0)/3$, TE. Same caption as in Fig. 12.

Let $v > 0$ and $\theta \in [0, 2\pi]$ denote the radial and angular elliptic coordinates: $x = c\cosh v\cos\theta$, $y = c\sinh v\sin\theta$. Adopting the same conventions than in [25,26],

$$e^{ik_0 x} = \sum_{m=0}^{+\infty} a_m^{inc} Je_m(v) Se_m(\theta)$$

where $Je_m(.)$ is the even radial Mathieu function of the first kind, $Se_m(.)$ the even angular Mathieu function (to alleviate the notations, the $k_0 c$ dependence of these functions is suppressed throughout), and $a_m^{inc} = i^m\sqrt{8\pi}/Ne_m$ where $Ne_m = \int_0^{2\pi} Se_m^2(\theta)d\theta$ is defined by Eq. (4.9) in [26]. The exact scattered field $u^s(v,\theta)$ writes [25]:

$$\begin{aligned} &u^s(v,\theta) = \sum_{m=0}^{+\infty} b_m^{ex} He_m(v) Se_m(\theta); \quad b_m^{ex} = -a_m^{inc}/\varphi_m \\ &\text{TM}: \quad \varphi_m = \frac{He_m(v_0)}{Je_m(v_0)}; \qquad \text{TE}: \quad \varphi_m = \frac{He'_m(v_0)}{Je'_m(v_0)} \end{aligned} \tag{67}$$

$He_m(.)$ is the even radial Mathieu function of the third kind, $v_0 = arctanh(b_0/a_0)$ the radial coordinate on S_0, and the prime denotes differentiation with respect to v. The exact RCS is $RCS(\theta) = 10\log[2\pi|\sigma^{ex}(\theta)|^2]$ with $\sigma^{ex}(\theta) = \sum_{m=0}^{\infty} i^m b_m^{ex} Se_m(\theta)$. Note that

$$\begin{aligned} c \to 0: \quad & Je_m(v_0) \to \sqrt{\pi/2} J_m(k_0 a_0), \quad He_m(v_0) \to \sqrt{\pi/2} H_m(k_0 a_0) \\ & Je'_m(v_0) \to k_0 a_0 \sqrt{\pi/2} J'_m(k_0 a_0), \quad He'_m(v_0) \to k_0 a_0 \sqrt{\pi/2} H'_m(k_0 a_0) \\ & Se_m(\theta) \to e^{im\theta} \end{aligned} \tag{68}$$

and (67) yields (4) with $\epsilon = \mu = 1$ and $R_2 = a_0$ when the ellipse tends towards the circle of radius a_0.

Because $\partial_n = \partial_v/\tau(\theta)$ and $\partial_l^2 = \partial_\theta^2/\tau^2(\theta)$ with $\tau(\theta) = \sqrt{a_1^2\sin^2\theta + b_1^2\cos^2\theta}$, the general expression of $T^{\pm}$ on S_1, as defined in (55), writes:

$$T^{\pm} = \frac{\partial_v}{\tau(\theta)} \pm \left(v_1^{\pm} + v_2^{\pm} \frac{\partial_\theta^2}{\tau^2(\theta)} \right) \tag{69}$$

Let $v = v_1$ on S_1; then the closed-form solutions in Ω_1 and Ω_2 write

$$\begin{aligned} &v_0 \leqslant v \leqslant v_1: \quad u_1(v,\theta) = \sum_{m=0}^{+\infty} [a_{1m} Je_m(v) + b_{1m} He_m(v)] Se_m(\theta) \\ &v \geqslant v_1: \quad u_2(v,\theta) = \sum_{m=0}^{+\infty} [a_m^{inc} Je_m(v) + b_{2m} He_m(v)] Se_m(\theta) \end{aligned} \tag{70}$$

and, from the definition (7) of the TCs on S_1 (with $\omega_\ell = 1$) and the expression (69) of $T^{\pm}$, we get:

$$\begin{aligned}
&\sum_{m=0}^{+\infty}[a_{1m}^{\ell}Je'_m(v_1)+b_{1m}^{\ell}He'_m(v_1)]Se_m(\theta)\\
&\quad+\sum_{m=0}^{+\infty}[a_{1m}^{\ell}Je_m(v_1)+b_{1m}^{\ell}He_m(v_1)]\left[\tau(\theta)v_1^{+}Se_m(\theta)+\frac{v_2^{+}}{\tau(\theta)}Se''_m(\theta)\right]\\
&\quad=\sum_{m=0}^{+\infty}[a_m^{inc}Je'_m(v_1)+b_{2m}^{\ell-1}He'_m(v_1)]Se_m(\theta)\\
&\qquad+\sum_{m=0}^{+\infty}[a_m^{inc}Je_m(v_1)+b_{2m}^{\ell-1}He_m(v_1)]\left[\tau(\theta)v_1^{+}Se_m(\theta)+\frac{v_2^{+}}{\tau(\theta)}Se''_m(\theta)\right]\\
&\sum_{m=0}^{+\infty}[a_{1m}^{\ell}Je'_m(v_1)+b_{1m}^{\ell}He'_m(v_1)]Se_m(\theta)\\
&\quad-\sum_{m=0}^{+\infty}[a_{1m}^{\ell}Je_m(v_1)+b_{1m}^{\ell}He_m(v_1)]\left[\tau(\theta)v_1^{-}Se_m(\theta)+\frac{v_2^{-}}{\tau(\theta)}Se''_m(\theta)\right]\\
&\quad=\sum_{m=0}^{+\infty}[a_m^{inc}Je'_m(v_1)+b_{2m}^{\ell}He'_m(v_1)]Se_m(\theta)\\
&\qquad-\sum_{m=0}^{+\infty}[a_m^{inc}Je_m(v_1)+b_{2m}^{\ell}He_m(v_1)]\left[\tau(\theta)v_1^{-}Se_m(\theta)+\frac{v_2^{-}}{\tau(\theta)}Se''_m(\theta)\right]
\end{aligned}$$

$Se''_m(\theta)$ is the second order derivative of $Se_m(\theta)$ with respect to θ. Taking into account (1) that implies $a_{1m}^{\ell}+b_{1m}^{\ell}\varphi_m=0$, multiplying the above identities by $Se_n(\theta)$ and integrating over θ yields:

$$\begin{aligned}
&\mathbf{F}\underline{b}_1^{\ell}+\underline{a}_1^{\ell}=0\\
&\mathbf{P}^{+}\underline{b}_1^{\ell}+\underline{a}_1^{\ell}-\mathbf{P}^{+}\underline{b}_2^{\ell-1}=\underline{a}^{inc}\\
&\mathbf{P}^{-}\underline{b}_1^{\ell}+\underline{a}_1^{\ell}-\mathbf{P}^{-}\underline{b}_2^{\ell}=\underline{a}^{inc}
\end{aligned}\tag{71}$$

$\underline{x}$ is a vector with components x_m, and boldface letters are matrices defined as follows:

$$\begin{aligned}
&\mathbf{F}_{mn}=\delta_{mn}\varphi_m,\quad \mathbf{P}^{\pm}=(\mathbf{J}^{\pm})^{-1}\mathbf{H}^{\pm}\\
&\mathbf{J}_{mn}^{\pm}=\delta_{mn}Je'_m(v_1)\pm\frac{S_{mn}^{\pm}}{Ne_m}Je_m(v_1),\quad \mathbf{H}_{mn}^{\pm}=\delta_{mn}He'_m(v_1)\pm\frac{S_{mn}^{\pm}}{Ne_m}He_m(v_1)\\
&S_{mn}^{\pm}=\int_0^{2\pi}\left[\tau(\theta)v_1^{\pm}Se_n(\theta)+\frac{v_2^{\pm}}{\tau(\theta)}Se''_n(\theta)\right]Se_m(\theta)d\theta
\end{aligned}\tag{72}$$

(δ_{mn} is the Kronecker symbol). When $c\to 0$, on account of (68), the expressions derived for the circular cylinder in the previous sections are recovered. Proceeding along the same lines as in Section 2.2, we set $\underline{u}_m=(b_{1m},a_{1m},b_{2m})^t$, $\underline{f}_m=(0,a_m^{inc},a_m^{inc})^t$ and the exact global system with the unknowns on the interfaces obtained from (71) writes $\mathbf{A}\underline{U}=\underline{F}$ where $\mathbf{A}$ is no more block-diagonal. Then, the block Gauss–Seidel iterative solution of the exact system $\mathbf{A}\underline{U}=\underline{F}$ with $\mathbf{A}=\mathbf{M}-\mathbf{N}$ and

$$\mathbf{M}=\begin{pmatrix}\mathbf{F}&\mathbf{I}&0\\ \mathbf{P}^{+}&\mathbf{I}&0\\ \mathbf{P}^{-}&\mathbf{I}&-\mathbf{P}^{-}\end{pmatrix}\quad \mathbf{N}=\begin{pmatrix}0&0&0\\ 0&0&\mathbf{P}^{+}\\ 0&0&0\end{pmatrix}\tag{73}$$

($\mathbf{I}$ is the identity matrix) is identical to the solution of (71): $\underline{U}^{\ell}=\mathbf{M}^{-1}\mathbf{N}\underline{U}^{\ell-1}+\mathbf{M}^{-1}\underline{F}$. The algorithm converges if and only if $\rho=\max|\lambda|<1$ where λ is an eigenvalue of $\mathbf{M}^{-1}\mathbf{N}$.

To minimize ρ, we first truncate, similarly to what is done in Section 3.2.1, the series in (70) to $Q+1$ terms ($0\leqslant m\leqslant Q$) and (44) with $R_2=a_0$ (i.e. the radius of the circumscribed circle to S_0) is still valid. Then we choose $v_1^{\pm}$ and $v_2^{\pm}$ to be θ independent so that the last identity in (72) writes:

$$S_{mn}^{\pm}=S_{mn}v_1^{\pm}+S''_{mn}v_2^{\pm}\tag{74}$$

If k_0a_0 is large enough, we have observed that the values of S_{mn}/S_{mm} and S''_{mn}/S''_{mm} are small if (i) $m\neq n$, (ii) m and n are large enough (the corresponding modes are evanescent) and (iii) the excentricity of S_1 is moderate (note that these matrices are diagonal when S_1 is a circle). If we make the approximation that matrices $\mathbf{S}^{\pm}$ are diagonal, then $\mathbf{A}$, $\mathbf{M}$ and $\mathbf{N}$ are block-diagonal and we can apply the procedure employed in Sections 4.1.4 and 4.2 to derive easily the following values of $v_1^{\pm},v_2^{\pm}$, that approximately minimize ρ. For the TC0 ($v_2^{\pm}=0$), $P_{mm}^{+}=0$ is the transpose of $\psi_{3m}^{+}=0$ and, from (72) and (74), the transpose of (52) is:

$$\mathrm{TC0}^{\pm}:\quad v_1^{+}=v_{1ap}^{+}=-\frac{1}{Q}\sum_{m=0}^{Q}\frac{He'_m(v_1)Ne_m}{He_m(v_1)S_{mm}}\quad v_1^{-}=v_{1ap}^{-}=ik_0\quad v_2^{\pm}=0\tag{75}$$

Similarly, the transpose of (60) for the TC2 is

$$\mathrm{TC2}^{\pm}: \quad v_1^{\pm} = v_{1ap}^{\pm}; \quad v_2^{+} = -\left[\frac{Ne_Q He'_Q(v_1)}{S''_{QQ} He_Q(v_1)} + v_{1ap}^{+}\frac{S_{QQ}}{S''_{QQ}}\right]; \quad v_2^{-} = \frac{i}{2k_0} \tag{76}$$

It is noteworthy that, as mentioned in Section 4.1.4, T^{+} in (69) with the above values of the coefficients can be used as an ABC. Finally, ρ is numerically computed for the standard zero order TC (TC0: $v_1^{\pm} = ik_0, v_2^{\pm} = 0$), the standard second order TC (TC2: $v_1^{\pm} = v_{31}, v_2^{\pm} = v_{32}$ as defined in (54) where $R_3 = R_1(\theta) = \tau^3(\theta)/(a_1 b_1)$ is the radius of curvature of S_1), and the improved TCs defined in (69), (75) and (76). It is important to note that ρ is computed from (72) with the exact non-diagonal matrices $\mathbf{S}^{\pm}$.

For $a_0 = 1m$, $b_0 = 0.5m$ and $f = 500$ MHz, Fig. 14 shows that the RCS calculated from (67) with the series truncated at $Q = 16$ [$\xi = 1.53$ in (44)] is in excellent agreement with the one computed from an integral equation or Method of Moments (MoM) code [27]. Fig. 15 plots ρ versus $(a_1 - a_0)/\lambda_0$ in TE (the creeping or evanescent waves are the strongest in this polarization, as

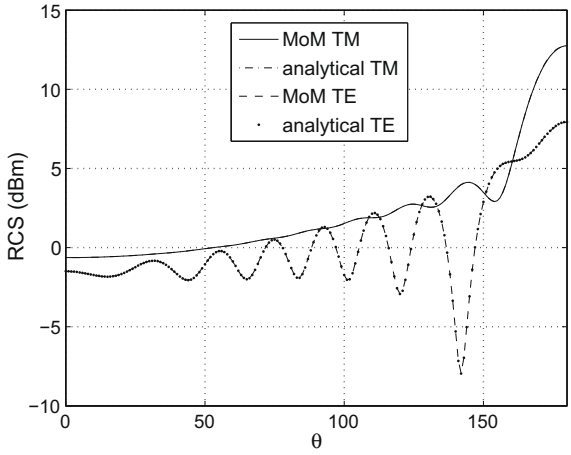

Fig. 14. PEC ellipse, $f = 500$ MHz, $a_0 = 1m$, $b_0 = 0.5m$: bistatic RCS versus θ computed from a MoM code and the analytical solution in (67) with the series truncated at $Q = 16$.

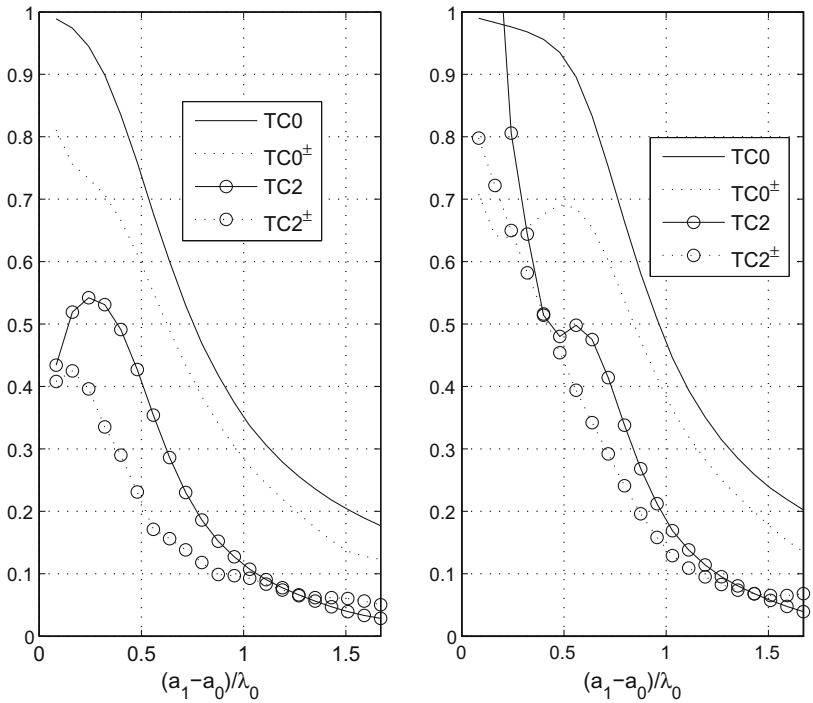

Fig. 15. PEC ellipse, $f = 500$ MHz, $a_0 = 1m$, $Q = 16$, TE: ρ versus $(a_1 - a_0)/\lambda_0$. Left: $b_0 = 1m$ (circle). Right: $b_0 = 0.5m$ (ellipse). TC0, TC2: ρ computed with the standard zero and second order TCs as defined in (69) and (54) for the TC2, with $v_{31} = ik_0$, $v_{32} = 0$ for the TC0. TC0$^{\pm}$, TC2$^{\pm}$: ρ computed with the improved zero and second order TCs as defined in (69), (75) and (76).

illustrated by the oscillations of the RCS in Fig. 14) for the above mentioned TCs, the circle $b_0 = a_0 = 1m$ and the above ellipse. It shows that the improved TCs perform always better than the standard ones (better results, not shown, are obtained in TM). We observe that ρ has similar values for the circle and the ellipse when a_1 is large. This comes from the fact that, as a_1 increases, S_1 tends towards the circle of radius a_1. Also, in view of (24), we conclude that the easy to implement TC0$^{\pm}$ is sufficient to obtain a rapid convergence rate. Finally, because the numerical values of $v_{1ap}^{+''}$ in (75) are positive ($5 < v_{1ap}^{+''} < 9.5$), the TC0$^{\pm}$ verify the uniqueness condition (49) for the above ellipse, unlike the TC2$^{\pm}$ for which v_{2ap}^{+} is also found to be strictly positive and, therefore, does not verify (58).

An important issue is the calculation of the various parameters $v^{\pm}$ when these TCs are implemented in an FEM. For the circular case analyzed in Sections 4.1.4 and 4.2, the only unknown parameter is Q, that might be evaluated as follows. Let R denote the radius of S_0 (or S_2 if a material coating is present). The mode of number Q is taken into account in an FEM calculation if $e^{iQ\theta}$ is correctly discretized on the circle of radius R. Assuming a uniform mesh of this circle, this entails that the angular separation between two adjacent nodes is $\delta\theta = 2\pi/(Qn_\theta)$ where n_θ is the number of discretization points required to represent $e^{iQ\theta}$ over a period $2\pi/Q$. If h denotes the length of an element, then $h = R\delta\theta$, that implies

$$Q = \frac{2\pi R}{h n_\theta} \tag{77}$$

Since $Q \simeq k_0 R$ because of (44), (77) yields $h \simeq \lambda_0/n_\theta$, and $n_\theta \simeq 10$ generally guarantees a good accuracy. If S_0 is not a circle, then (77) still holds if R is the radius of the circumscribed circle to S_0 (or S_2), as verified by the results presented above for the PEC ellipse. For an arbitrary shape of the interfaces, the simple solution that consists in substituting in (52) and (60) the local radii of curvature to the radii of the interfaces is efficient only if these interfaces are almost circular. Indeed, for the ellipse considered above, we have found that the value of ρ computed for the TC0$^{\pm}$ with $v_1^{+} = v_{1ap}^{+}$ as defined in (52) where $Q = 16$ and $R_3 = R_1(\theta)$ is close to the one plotted in Fig. 15 when a_1 is large, but is larger than one when $(a_1 - a_0)/\lambda_0 \leqslant 0.37$.

Note that the more complex case of a coated elliptical PEC cylinder may be investigated by using the analytical solutions defined, e.g., in [28], and following along the same lines. However, this is beyond the scope of this paper.

7. Conclusions

The study of this model problem has allowed to draw, or to confirm, the following results. First, from a general point of view:

- The performances of the block Gauss–Seidel preconditioner utilized in [10] for the solution of the global system increase with those of the TCs.
- The efficiency of the TCs (or, equivalently, the convergence rate of the DDM) decreases when the numerical accuracy (here governed by Q) increases.
- It has been analytically verified on two examples that Després' algorithm (Jacobi) converges less rapidly than the one in [15] (Gauss–Seidel).
- For a given TC, the latter converges all the faster since losses in the material are large.
- The analytical expressions of ρ and the numerical results show that ρ may be reduced if S_3 is moved farther away from the object.
- The relaxed algorithm employed in [15,16] with standard Robin TCs is much less efficient than the non-relaxed one implemented with the improved TCs.
- The impact on the convergence rate of an additional interface located inside the material has been quantified.
- Except when the interface is located in free-space, coefficients $v_m^{\pm}$ in the approximate TCs presented in Sections 3 and 4 are polarization dependent. This entails that a TC, that relates, on an interface and in, e.g, an H-formulation, $\underline{n} \times \underline{E}$ and $\underline{n} \times \underline{n} \times \underline{H}$, involves a (2×2) diagonal operator when written in the orthonormal basis constituted by the vectors tangent to the principal lines of curvature of the interfaces, similarly to the anisotropic second order TC implemented in [16].

Second, regarding the TCs, and in order of increasing efficiency and difficulty of implementation:

- The zero order (local) TCs in [17,19] investigated in Section 3 are efficient only if $v' \neq 0$. Uniqueness of the solutions in each SD is guaranteed if $v'' \geqslant 0$, but sufficient conditions of convergence (SCC) have not been obtained when $v' \neq 0$, except when $\epsilon'\mu' < 0$, in which case convergence is fast, even for a lossless material.
- Like the above TCs, no SCC has been derived for the local ones presented in Section 4.1 with $v^{+} \neq v^{-}$. If $\epsilon, \mu \in \mathbb{R}$, uniqueness of the solutions is guaranteed in each SD for the approximate values, $v_{1,3ap}^{\pm}$, of $v_{1,3}^{\pm}$ that minimize ρ (this issue remains open when $\epsilon, \mu \in \mathbb{C}$). By utilizing Debye's asymptotic expansion, we have provided a geometric interpretation of v_{3ap}^{+} when S_3 is outside of the evanescent region, that may also be used in a local ABC. Applying similar asymptotic expansions when S_3 is close to S_2, or to coefficients $v_1^{\pm}$ involved in the TCs prescribed inside the material may be considered, but this is beyond the scope of this paper.
- The non-local TC2s proposed in Section 4.2 ($v^{+} \neq v^{-}$ and are m dependent) speed up the convergence. However, neither the convergence, nor the uniqueness of the solutions in each SD, are guaranteed.

Finally, the generalization to surfaces of more general shape has been tackled in Section 6 (elliptical cylinders), and an estimation of Q from an FE mesh has been proposed. The extension of this approach to 3D applications using spherical and, tentatively, spheroidal surfaces may be considered in a future work at the cost, however, of increased analytical and computational complexities.

Appendix A. Proof of (35)

The first identity in (7) with $\omega_\ell = \omega$ yields

$$\begin{aligned} &E^\ell \leqslant |1-\omega|^2 E^{\ell-1} + |\omega|^2 \int_{S_1} |T^+ e_2^{\ell-1}|^2 \\ &\omega = 1: \quad E^\ell = \int_{S_1} |T^+ e_2^{\ell-1}|^2 \end{aligned} \tag{78}$$

(34) and the two first identities in (7) give, on S_1 and for $i = 1,2$:

$$|T^+ e_i^{\ell-1}|^2 = |T^- e_i^{\ell-1}|^2 + 4\Re\left(v_1^* e_i^{(\ell-1)*} \frac{\partial_n e_i^{\ell-1}}{\epsilon} \right) \tag{79}$$

Because $T^- e_2^{\ell-1} = T^- e_1^{\ell-1}$ [see (7)], (79) implies, for $i = 2$,

$$|T^+ e_2^{\ell-1}|^2 = |T^- e_1^{\ell-1}|^2 + 4\Re\left(v_1^* e_2^{(\ell-1)*} \frac{\partial_n e_2^{\ell-1}}{\epsilon} \right)$$

Similarly, (79) with $i = 1$ entails

$$|T^- e_1^{\ell-1}|^2 = |T^+ e_1^{\ell-1}|^2 - 4\Re\left(v_1^* e_1^{(\ell-1)*} \frac{\partial_n e_1^{\ell-1}}{\epsilon} \right)$$

and

$$|T^+ e_2^{\ell-1}|^2 = |T^+ e_1^{\ell-1}|^2 + 4\Re\left(v_1^* e_2^{(\ell-1)*} \frac{\partial_n e_2^{\ell-1}}{\epsilon} - v_1^* e_1^{(\ell-1)*} \frac{\partial_n e_1^{\ell-1}}{\epsilon} \right)$$

Finally, since $E^{\ell-1} = \int_{S_1} |T^+ e_1^{\ell-1}|^2$ [see (35)], (78) writes:

$$E^\ell \leqslant (|\omega|^2 + |1-\omega|^2) E^{\ell-1} + 4|\omega|^2 Re\left\{ v_1^* \int_{S_1} e_2^{(\ell-1)*} \frac{\partial_n e_2^{\ell-1}}{\epsilon} - v_1^* \int_{S_1} e_1^{(\ell-1)*} \frac{\partial_n e_1^{\ell-1}}{\epsilon} \right\} \tag{80}$$

(the inequality becomes an equality when $\omega = 1$). On the other hand, on account of (1) and (33), the energy conservation derived from Maxwell's equations (see, e.g., [24]) entails, if $\underline{E}_i^\ell$, $\underline{H}_i^\ell$ designate the difference with the exact fields of the fields computed at iteration ℓ,

$$\begin{aligned} A_1^\ell &= k_0^2 \int_{\Omega_1} [\epsilon^* |\underline{E}_1^\ell|^2 - \mu |\underline{H}_1^\ell|^2] = \int_{S_1} e_1^{\ell *} \frac{\partial_n e_1^\ell}{\epsilon} \\ A_2^\ell &= k_0^2 \int_{\Omega_2} [\epsilon^* |\underline{E}_2^\ell|^2 - \mu |\underline{H}_2^\ell|^2] = -\int_{S_1} e_2^{\ell *} \frac{\partial_n e_2^\ell}{\epsilon} - v_1 \int_{S_2} |e_2^\ell|^2 \end{aligned} \tag{81}$$

and (80), (81) imply (35).

Appendix B. Justification of (50) and (51)

We attempt to minimize the numerator $(\psi_{1m}^- - \varphi_m)(\psi_{1m}^+ - r_m^\infty)$ of λ_m in (31). This is exactly realized by the first identity in (27) provided that the denominator of v_{1m}^-, that is proportional to $D(m)$,

$$\begin{aligned} &\text{TM}: \quad D(m) = J_m(kR_1) H_m(kR_0) - H_m(kR_1) J_m(kR_0) \\ &\text{TE}: \quad D(m) = J_m(kR_1) H'_m(kR_0) - H_m(kR_1) J'_m(kR_0) \end{aligned} \tag{82}$$

is non-zero for $0 \leqslant m \leqslant Q$. Then, v_{1m}^- varies continuously with m, and we have observed numerically that $|\psi_{1Q}^- - \varphi_Q| \simeq 0$ minimizes ρ. Regarding v_{1ap}^+, we have observed numerically that the average value in $[0,Q]$ of v_{1m}^+ defined by (27) yields a good approximation of the optimum value of v_1^+.

When there exists $x \in [0,Q]$ such that $D(x) = 0$, then v_{1m}^- displays a quasi-resonance in $[0,Q]$ (m is an integer) and (50) yields bad results. In this case, we have observed numerically that $|\psi_{1Q}^+ - r_Q^\infty| \simeq 0$ minimizes ρ and that this minimum depends but weakly on v_1^-. As a consequence, we choose $v_{1ap}^- = ik_0$ that yields good results and satisfies (49).

For a lossy material, $D(m) \in \mathbb{C}$ and it is unlikely that $D(x) = 0$ if $x \in [0,Q]$. Conversely ($\epsilon, \mu \in \mathbb{R}$), because $H_m(x) = J_m(x) - iY_m(x)$, $\Re[D(m)] = 0$ and $D(m)$ may be zero for $m \ll |k|R_0 < |k|R_1$. Actually, the asymptotic expansions of $H_m(x)$ and $J_m(x)$ in $O(x^{-1/2})$ and for $m \ll x$ yield [22]

$$\text{TM}: \quad D(m) \simeq \frac{2i}{\pi k\sqrt{R_1 R_0}} \sin[k(R_1 - R_0)]; \qquad \text{TE}: \quad D(m) \simeq \frac{2i}{\pi k\sqrt{R_1 R_0}} \cos[k(R_1 - R_0)]$$

and

$$D(m) \simeq 0 \Longleftrightarrow \text{TM}: \quad R_1 - R_0 = p\lambda/2; \qquad \text{TE}: \quad R_1 - R_0 = (2p+1)\lambda/4; \quad p \in \mathbb{N} \tag{83}$$

Appendix C. Derivation of (53)

If the sum in (52) is approximated by a integral on m, we get:

$$v_{3ap}^{+} \simeq -\frac{k_0}{Q} \int_0^Q \frac{H_m'(k_0 R_3)}{H_m(k_0 R_3)} dm \tag{84}$$

From (44), $Q \simeq k_0 R_2$, and $x = k_0 R_3 > m + O(m^{1/3})\ \forall m \leqslant Q$ if x is large enough, in which case Debye's asymptotic approximation [22] can be used

$$\begin{aligned} H_m(x) &\simeq \sqrt{\frac{2}{\pi x \sin\kappa(m)}} e^{ix[\kappa(m)\cos\kappa(m) - \sin\kappa(m)] + i\pi/4} \left[1 + \frac{ig(m)}{x\sin\kappa(m)} + O(x\sin\kappa(m))^{-2}\right] \\ \sin\kappa(m) &= \sqrt{1 - m^2/(k_0 R_3)^2} \quad g(m) = \frac{1}{8} + \frac{5}{24\tan^2\kappa(m)} \end{aligned} \tag{85}$$

that entails

$$\frac{H_m'(x)}{H_m(x)} \simeq -\left[\frac{1}{2x\sin^2\kappa(m)} + i\sin\kappa(m)\right] + O(x\sin\kappa(m))^{-2} \tag{86}$$

Reporting this expression into (84), we get (53).

References

[1] B. Stupfel, B. Després, A domain decomposition method for the solution of large electromagnetic scattering problems, J. Electromagn. Waves Appl. 13 (1999) 1553–1568.
[2] B. Stupfel, A hybrid finite element and integral equation domain decomposition method for the solution of the 3D scattering problem, J. Comput. Phys. 172 (2001) 451–471.
[3] K. Mer-Nkonga, M. Mandallena, D. Goudin, B. Stupfel, F. Collino, A numerical strategy for a high frequency electromagnetic scattering problem in a mixed formulation, C.R. Phys. 7 (2006) 509–517.
[4] B. Després, P. Joly, J.E. Roberts, A domain decomposition method for the harmonic Maxwell equations, in: R. Beauwens, P. de Groen (Eds.), Iterative Methods in Linear Algebra, Elsevier Science Pub., 1992, pp. 475–484.
[5] C. Farhat, F.X. Roux, A method of finite element tearing and interconnecting and its parallel solution algorithm, Int. J. Numer. Methods Eng. 32 (1991) 1205–1227.
[6] B. Després, Domain decomposition method and the Helmholtz problem (part II), in: Proceedings of the International Symposium on Mathematical and Numerical Aspects of Wave Propagation, SIAM, 1993, pp. 197–206.
[7] F. Collino, S. Ghanemi, P. Joly, Domain decomposition method for harmonic wave propagation: a general presentation, Comput. Methods Appl. Mech. Eng. 184 (2000) 171–211.
[8] F. Magoulès, F.X. Roux, S. Salmon, Optimized discrete transmission conditions for a non-overlapping domain decomposition method for the Helmholtz equation, SIAM J. Sci. Comput. 25 (5) (2004) 1497–1515.
[9] S.C. Lee, M.N. Vouvakis, J.F. Lee, A non-overlapping domain decomposition method with non-matching grids for modeling large finite antenna arrays, J. Comput. Phys. 203 (2005) 1–21.
[10] K. Zhao, V. Rawat, S.C. Lee, J.F. Lee, A domain decomposition method with nonconformal meshes for finite periodic and semi-periodic structures, IEEE Trans. Antennas Propagat. 55 (9) (2007) 2559–2570.
[11] Y.J. Li, J.M. Jin, A new dual-primal domain decomposition approach for finite element simulation of 3D large-scale electromagnetic problems, IEEE Trans. Antennas Propagat. 55 (10) (2007) 2803–2810.
[12] Z.Q. Lu, X. An, W. Hong, A fast domain decomposition method for solving 3D large scale electromagnetic problems, IEEE Trans. Antennas Propagat. 56 (8) (2008) 2200–2210.
[13] J. Gaidamour, P. Hénon, A parallel direct/iterative solver based on a Schur complement approach, in: IEEE 11th International Conference on Computational Science and Engineering, Sao Paulo, Brazil, July 2008, pp. 98–105.
[14] B. Després, Méthodes de décomposition de domaines pour les problèmes de propagation d'ondes en régime harmonique, Thèse de Mathématiques Appliquées, Paris VI, 1991.
[15] B. Stupfel, A fast domain decomposition method for the solution of electromagnetic scattering by large objects, IEEE Trans. Antennas Propagat. 44 (10) (1996) 1375–1385.
[16] B. Stupfel, M. Mognot, A domain decomposition method for the vector wave equation, IEEE Trans. Antennas Propagat. 48 (5) (2000) 653–660.
[17] M.J. Gander, F. Magoulès, F. Nataf, Optimized Schwarz methods without overlap for the Helmholtz equation, SIAM J. Sci. Comput. 24 (1) (2002) 38–60.
[18] F.X. Roux, F. Magoulès, L. Series, Y. Boubendir, Approximation of optimal interface boundary conditions for two-Lagrange multiplier FETI method, in: Domain Decomposition Methods in Science and Engineering, Springer, 2005, pp. 283–290.
[19] Y. Boubendir, Techniques de décomposition de domaines et méthodes d'équations intégrales, Thèse de Mathématiques Appliquées, INSA Toulouse, 2002.
[20] O.M. Bucci, G. Franceschetti, On the degrees of freedom of scattered fields, IEEE Trans. Antennas Propagat. AP-37 (1989) 918–926.

[21] B. Stupfel, Y. Morel, Singular value decomposition of the radiation operator – application to model-order and far-field reduction, IEEE Trans. Antennas Propagat. 56 (6) (2008) 1605–1615.
[22] G.N. Watson, A Treatise on the Theory of Bessel Functions, Cambridge Univ. Press, 1944.
[23] F. Magoulès, P. Ivanyi, B.H.V. Topping, Non-overlapping Schwarz methods with optimized transmission conditions for the Helmholtz equation, Comput. Methods Appl. Mech. Eng. 193 (2004) 4797–4818.
[24] J.C. Nédélec, Acoustic and electromagnetic equations. Integral representations for harmonic problems, Applied Mathematical Sciences 144 (2000).
[25] J.J. Stamnes, Exact two-dimensional scattering by perfectly reflecting elliptical cylinders, strips and slits, Pure Appl. Opt. 4 (1995) 841–855.
[26] J.J. Stamnes, B. Spjelkavik, New method for computing eigenfunctions (Mathieu functions) for scattering by elliptical cylinders, Pure Appl. Opt. 4 (1995) 251–262.
[27] P. Bonnemason, B. Stupfel, Technical report, CEA, DAM, CEL-V, 1992.
[28] A.R. Sebak, Scattering from dielectric-coated impedance elliptic cylinder, IEEE Trans. Antennas Propagat. 48 (10) (2000) 1574–1580.